Master's thesis

NTNU
Norwegian University of Science and Technology
Faculty of Natural Sciences
Department of Materials Science and Engineering

Yukihiro Takahashi

Carbon Capture and Recovery by Molten Salts Electrochemistry

Master's thesis in Materials Science and Engineering
Supervisor: Geir Martin Haarberg
Co-supervisor: Espen Sandnes
June 2022

NTNU
Kunnskap for en bedre verden

Yukihiro Takahashi

Carbon Capture and Recovery by Molten Salts Electrochemistry

Master's thesis in Materials Science and Engineering
Supervisor: Geir Martin Haarberg
Co-supervisor: Espen Sandnes
June 2022

Norwegian University of Science and Technology
Faculty of Natural Sciences
Department of Materials Science and Engineering

NTNU
Norwegian University of
Science and Technology

Preface

At some point when I was a small boy, I vaguely learned the existence of something called "global warming", which is happening all over the world. It makes the world hotter and hotter, and polar bears are in danger. Also, I was taught that the culprit is something in the air, named "carbon dioxide". Then, I thought, "Why don't adults just catch and punish them?".

As I grew up and started studying some science, I realised that it is really a difficult job to do (particularly to punish them). But now, at least, I have learnt one of the possibilities to catch and reuse them by using molten salt electrochemistry. In my opinion, the most exciting thing about electrochemistry is that it allows us to achieve reactions that never happen spontaneously. A glass of water does not suddenly evolve hydrogen and oxygen, and CO_2 in the air cannot be turned into carbon powder and oxygen, as long as we leave it alone. But this is something we humans can.

This master's thesis was written as a continuity of TMT4500, Specialisation project offered by the Department of Materials Science and Engineering at NTNU. The author has been working on the same topic, "Carbon Capture and Recovery by Molten Salts Electrochemistry" throughout the year. The results obtained during the second half of the year are summarised here.

This thesis provides insights into the possibility of CO_2 electrolysis in molten $CaCl_2$-based salt systems. As this work has had an aspect as a startup of this kind of research ever in the present research group, the study has been advancing with numerous trials, errors, and sometimes, disappointments. Nevertheless, the author is sure that the series of the studies has been fruitful, and the base for the next steps has successfully been established. Although no one is yet sure if this technology is truly feasible in industry and is able to contribute to addressing the environmental problems, this topic will be worth to be continued for our future.

Last but not least, I would like to express my gratitude to my co-supervisor and main supervisor, Associate professor Espen Sandnes and Professor Geir Martin Haarberg. This year's experience has been genuinely wonderful and enjoyable for me. They have been always motivating and have given me new perspectives. It has been a great pleasure to work with them. Although I am starting working for a different topic and project under different supervisors, I wish we could continue to collaborate together from time to time.

Y. Takahashi
June 2022

Abstract

To mitigate global warming and climate change, it is an urgent mission for us to reduce the amount of CO_2 in the atmosphere. One of the viable solutions to this challenge may be to capture, and preferably, to recover CO_2 from gas phases. It has been reported that CO_2 gas can be captured and decomposed into elemental carbon and oxygen by molten salt electrolysis. In this study, CO_2 splitting in molten $CaCl_2$-NaCl-$CaCO_3$ was explored. Although this $CaCl_2$-based salt system has many advantages such as the low cost and abundance of the materials, there are limited numbers of studies, and the understanding of the process is still insufficient. To provide some insights into it, the following things were investigated. First, the cathodic behaviour of carbonate in the melt was studied. Voltammetric studies revealed that the reduction process was happening in either one step or two steps depending on the electrode materials. The nucleation process of carbon was studied, and the diffusion coefficient of carbonate ion was determined from the current transient. Second, the feasibility of inert anodes in the process was examined. An SnO_2-based anode showed a good performance and stability in the present molten salt system for a long time. Finally, voltammetric and electrolytic studies using actual CO_2 gas were carried out. Pure or diluted (1 vol%) CO_2 gas was injected into the system as the carbon source. In either case, the deposition of carbon on the cathode was confirmed.

Table of contents

1 Introduction

1.1 Background and motivation

Global warming and climate change are huge concerns for all of us human beings. The origin of this crisis has been attributed to the emissions of greenhouse gasses (GHGs), which have been emitted through our activities such as the use of fossil fuels. The gasses are accumulated in the air, and they are now causing the notorious "greenhouse effect". The average temperature on earth has risen due to anthropogenic activities after the industrial revolution. Fig. 1.1 shows the change in the global surface temperature[1]. Here, if the yearly average temperature is higher than the average temperature from 1901 to 2000, it is represented as a red bar, whereas if it is lower, the colour is blue. This figure clearly demonstrates that the surface temperature on earth has increased within the last 100 years.

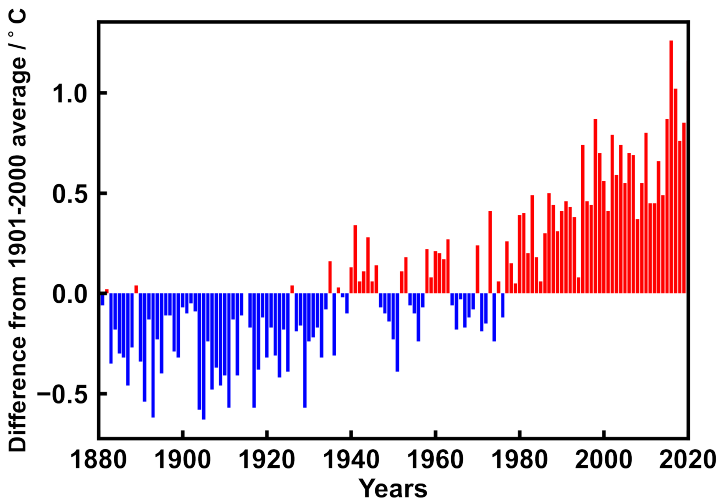

Figure 1.1. Yearly surface temperature difference from the average from 1880 to 2020.[1]

The temperature rise causes a lot of detrimental consequences for us. One of the most famous examples may be the sea-level rise. IPCC (Intergovernmental Panel on Climate Change) is anticipating that the global mean sea level (GMSL) will rise between 0.43 m and 0.84 m by 2100, depending on the scenario.[2] Other effects of global warming include severe and unprecedented weather, drought, forest fires, and many others. Each of them gives huge impact on all the organisms on earth as well as mankind.

In order to mitigate these unfavourable changes, it is necessary for us to develop new technologies to decrease the amount of GHGs in the atmosphere. There are two approaches to tackle this challenge. First, it is effective to replace our conventional processes that release GHGs with ones that release less amount of such

gasses. This kind of approach is the most common these days.

The other approach is to capture GHGs from the atmosphere. Although this approach is extremely challenging with the current knowledge and technologies, it is a highly desirable way to further decelerate the pace of climate change.

Among many kinds of GHGs, the contribution of CO_2 occupies a large percentage. The emission of CO_2 accounts for 76% of all the greenhouse gasses.[3] Since CO_2 is a chemically stable gas, it can be easily produced through various processes. Figure 1.2a shows the global emission of CO_2.[4] The amount of CO_2 emitted per year has been drastically increased over the last century and it is now around 35 billion tons annually. As a result, the concentration of CO_2 has risen and reached 420 ppm in April 2022.[5] It is worth noting that the average CO_2 concentration was below 300 ppm over 800,000 years before the modern period.[6], [7] Therefore, it is an urgent mission to establish effective and viable ways to reduce the amount of CO_2 in the atmosphere.

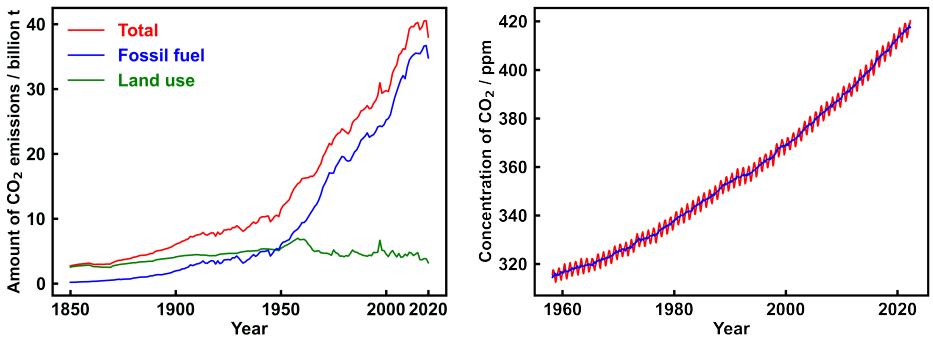

Figure 1.2. (a)Amounts of global CO_2 emission[4] and (b)atmospheric CO_2 concentrations measured at Mauna Loa[5].

As for CO_2 emissions, the use of fossil fuels has been attributed to be the biggest factor. They have been used as our convenient energy sources for a long time. These days, there are many kinds of ongoing research and development of renewable energy sources to replace fossil fuels. Such technologies, for instance, include solar, wind, hydropower, geothermal, and biomass. The problems of these alternatives are mainly the following points: huge costs for the processes or the construction, unreliability due to the intermittency, and strong dependency on the geographical situation. Due to the uncertainty of these renewable energies, they have not successfully replaced the conventional energy sources.

The utilisation of other carbon-containing species is another cause. Carbon materials have widely been employed for our industrial processes. For example, carbon electrodes are used as an anode in aluminium electrolysis. Despite the fact that it emits a huge amount of CO_2 from the process, this method is still the only economical way to produce aluminium. The reason is attributed to the advantageous properties that carbon materials have, such as the good electrical conductivity, high chemical stability, mechanical strengths, and costs. Similarly, in other industrial processes, as long as the advantages of use of carbon outweighs the drawbacks, carbon materials will still continue to be needed.

In these ways, the availability, reliability, and versatility of carbon materials have made it difficult for us to remove all the carbon-containing species from our lives immediately. Therefore, one can easily imagine that the current situation where fossil fuels and carbon materials are widely used will persist for a while.

Based on the current situation and challenges regarding the use of carbons, one of the realistic ways to stop climate change may be to capture CO_2 from the atmosphere, rather than prohibiting all the usage of carbon in near future.

One of the probable technologies to retrieve CO_2 is called Carbon Capture and Storage (CCS) technology.[8]–[10] The main idea is that CO_2 gas is collected from a gas phase, and it is concentrated and compressed. Then, it is transported to places far away from the atmosphere, such as the bottom of deep oceans or deep underground, and stored there. However, it is not necessarily easy to obtain concentrated CO_2 gas from various industrial processes, and therefore, a lot of extra energy and complicated processes are usually required for the separation step. Another drawback is the potential risk of the leakage into the atmosphere. So, even though a considerable amount of efforts have been made in this area, it has not become an ultimate solution to the CO_2 and environmental problems.

Another possibility is to decompose CO_2 into other carbon-containing materials. For instance, electrolytic or photoelectrolytic reduction of CO_2 in aqueous media has been extensively studied so far.[11]–[13] One of the advantages of this process is the variety of products including alcohols, aldehydes, carboxylic acids, CO, and even hydrocarbons. These materials are important raw materials in chemical industries and it is beneficial to synthesise such chemicals from CO_2. In addition, this process can also be regarded as an energy storage process where electric or light energy is converted into chemical energy. The fact that it can give us many kinds of products can also be a drawback. It is the difficulty to improve the selectivity of the desired product and maximise the yield. Since most of the products remain in aqueous media, it is always challenging to separate them in an efficient and economical manner. The poor solubility of CO_2 gas in water is another issue. The solubility of CO_2 in water at 298 K is only 1.45 g/kg_{water}.[14] Furthermore, the biggest challenge is the presence of water as a medium. Since water splitting reaction is thermodynamically and kinetically favoured over CO_2 reduction reac-

tions, it leads to H_2 evolution rather than the production of desired materials.

To address these drawbacks, inorganic molten salts are attractive reaction media for CO_2 electrolysis. They have high solubility of CO_2, high chemical stability, and wide potential windows. The high-temperature environment is also advantageous to promote kinetically challenging reactions, where the severing of strong C=O bonds is required. This can lead to reducing the cost of the electrode materials, as high reaction rates can be achieved even without expensive catalytic metals such as Pt.

In molten salt systems, due to absence of water, CO_2 can be directly split into elemental carbon and oxygen by the following reaction.

$$CO_2(g) \rightarrow C + O_2(g) \tag{1}$$

This reaction is significant as it can contribute not only to dealing with the greenhouse gas, but also to producing useful carbon materials out of it. The by-product, oxygen, is also an important substance for industrial and medical usage. However, this electrolytic CO_2 splitting has not attracted so much attention and not yet applied to the industry. On the contrary, it has been regarded as one of the unwanted side reactions in metal production processes in molten salt, as the carbon can contaminate the products.[15] Other possible reasons why it has not been so popular would be the wide availability of various carbon materials made from fossil fuels and the lack of understanding of the processes. But now, the development of new sustainable synthesis routes is strongly hoped all over the world, and the demand for new production methods of carbon materials including carbon nanomaterials has been largely increased. This CO_2 splitting reaction has a potential to meet such new demands as well. Thus, in order to address the environmental issues and to find novel production routes for carbon materials, electro-decomposition of CO_2 in molten salts is a key technology to be developed.

Nowadays, there are many publications regarding CO_2 electrolysis in molten salt. [16]–[20] As it will be introduced in 2.1.2, one of the most attractive points of this electrolytic carbon deposition process is that the products can be a variety of carbon materials, including amorphous carbons, carbon nanotubes(CNTs)/fibres (CNFs), graphenes, and many other forms. In order to control the final product, the selection of the reaction condition is hugely important. Particularly, the choice of the electrolyte affects the whole reaction conditions, as it determines the solubility of CO_2, liquidus temperature and many others.

While Li_2CO_3-based molten salt systems have been widely investigated as an electrolyte for CO_2 electrolysis, owing to their thermodynamical stabilities and low liquidus temperatures[16], [19], $CaCl_2$-based molten salt is also an attractive electrolyte. There are three advantages to this salt. First, $CaCl_2$ is stable and has a fairly wide potential window. Second, $CaCl_2$ shows a good solubility of several

oxides such as CaO[21], which is an absorbent of CO_2 gas. Third, calcium chloride is a cheap and safe material. For these reasons, a $CaCl_2$-NaCl-CaO(or $CaCO_3$) molten salt system was chosen as an electrolyte in this study. Here, $CaCl_2$ is a base electrolyte. NaCl plays roles to lower the liquidus temperature [21] and improve the conductivity of the melt [22]. It also contributes to decreasing the hygroscopicity and the viscosity of the melt. CaO takes a role as a capturing agent of CO_2 gas, in the form of $CaCO_3$.

In spite of the benefits of the $CaCl_2$-based molten salts, the number of publications of CO_2 electrolysis in $CaCl_2$-based molten salts is still limited, and therefore, the understanding of the processes is not as sufficient as that of other electrolytes such as Li_2CO_3 systems. In addition to the advantageous physical and electrochemical properties described above, the abundance of the electrolyte materials can be a big advantage considering the amount of lithium resources on earth and the instability of the supply chain. Thus, CO_2 decomposition in molten $CaCl_2$ systems is an important topic to be investigated to make the CO_2 electrolysis process feasible and to realise the carbon capture and recovery technology.

1.2 Aim and scope of the work

The biggest aim is to provide new insights into CO_2 electrolysis in $CaCl_2$-based molten salt so as to contribute to the realisation of the carbon capture and recovery technology using molten salts. To approach this, the following topics were chosen as the objectives of this thesis work: (i) Elucidation of cathodic behaviour of carbonate, (ii) Confirming the feasibility of inert anodes, and (iii) Use of simulated exhausts as the carbon source.

The first objective is to investigate the cathodic behaviour of carbonate and dissolved CO_2 in the $CaCl_2$-NaCl-CaO molten salt system. Even though some studies have shown that the electrodeposition of carbon in $CaCl_2$-based molten salts is possible, the focus has been mainly on the experimental conditions and carbon product itself. Thus, sufficient attention has not necessarily been paid to the reaction mechanisms and other electrochemical aspects, such as the nucleation process or the diffusion coefficient. In this study, voltammetry of molten $CaCl_2$-NaCl-$CaCO_3$ (or CaO) was performed employing several different cathode materials. The reaction mechanisms of carbon deposition process from carbonate will be discussed. Besides, the nucleation process of carbon on the cathode was studied by using potential step techniques. The diffusion coefficient of carbonate ions was also estimated from the current transient.

Secondly, the application of inert anodes to the process is of a great importance. While carbon-based anodes such as graphite or glassy carbon are convenient for fundamental studies, it is not ideal as it can produce CO_2 or CO through side reactions and can be consumed during the process. Since O_2 is produced at the

anode during the carbon deposition reaction, oxidation of carbon can easily happen at high temperatures above 500 °C.

$$C + O_2(g) = CO_2(g) \tag{2}$$

Also, under an atmosphere containing CO_2, Boudouard reaction can also take place.

$$C + CO_2(g) = 2CO(g) \tag{3}$$

These reactions lead to the loss of the electrode material and it means frequent replacement of electrodes can be required during the process, which is an inconvenient feature when applied to the industry. More importantly, emitting CO_2 is obviously far from ideal since the aim of the electro-splitting of CO_2 is to capture and reduce CO_2. In this study, an SnO_2-based anode was investigated as an inert anode candidate. SnO_2 has been known as a stable electrode material in various halide molten salts.[23] It shows a fairly good electrical conductivity and durability against thermal shock. However, since the solubility and other behaviours of anode materials are largely different from system to system, it is necessary to test the feasibility in the present molten salt system as well. The stability as an inert anode was studied by long-term electrolysis with a comparison to the results obtained in the previous study (TMT4500: Specialisation project [24]) where a Ni-based alloy anode was attempted.

Finally, aiming at the application to various industrial processes, it is important to investigate the electro-deposition of carbon by using actual CO_2 gas as the carbon source. The use of carbonate ions can be considered to be mostly sufficient to simulate the situation where CO_2 is dissolved in the molten salt. But it is still not a real condition and not ideal. In this thesis, the cathodic process was investigated by potential sweep methods under simulated exhaust from industrial processes containing CO_2. Instead of $CaCO_3$, CaO was added as an absorbent of CO_2 gas. The role of oxide ions in the melt was also studied by blank experiments. Based on the results of voltammetry, potentiostatic electrolysis under CO_2 gas flow was performed. A diluted CO_2 gas was also employed in addition to pure CO_2. Although pure CO_2 gas might be ideal in terms of the supply of CO_2, the real CO_2 concentration from various processes are much lower. For instance, a typical CO_2 concentration of exhaust from aluminium electrolysis is about 1%. The concentration cannot be easily increased without extra energy and processes. So, it is important to confirm the feasibility of using a diluted CO_2 gas as the carbon source. The effect of different concentrations on the carbon deposition process is discussed.

2 Theory

2.1 Electrolytic CO_2 splitting in molten salts

2.1.1 Carbon deposition reaction from carbonates

Figure 2.1 shows the overview of CO_2 splitting in a molten salt. The cell consists of an electrolyte, an anode, a cathode, and a power source. When CO_2 gas is supplied to the molten salt system containing oxide ions, CO_2 molecules can be converted to carbonate ions by the following reaction:

$$CO_2(g) + O^{2-} \rightleftarrows {CO_3}^{2-} \tag{4}$$

With an appropriate potential applied, the carbonate ions can be reduced into elemental carbon at the cathode. The carbon deposition reaction from carbonate ions can be expressed as follows:

$${CO_3}^{2-} + 4e^- \rightarrow C + 3O^{2-} \tag{5}$$

This is a one-step 4-electrons reaction and is the most widely accepted reaction formula for carbon deposition from carbonate. In addition to this, there are two more proposed reaction mechanisms.[25], [26] They are introduced in Appendix B.

At the same time, oxygen can be produced from oxide ions at the anode.

$$2\,O^{2-} \rightarrow O_2(g) + 4e^- \tag{6}$$

In total, CO_2 is electrolytically split into carbon and oxygen gas.

$$CO_2(g) \rightarrow C + O_2(g) \tag{7}$$

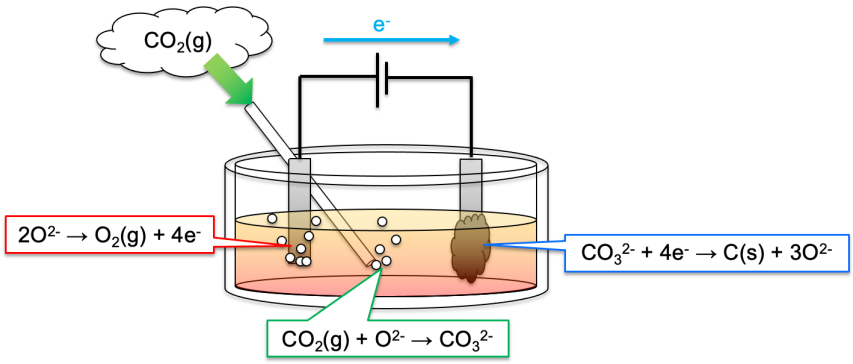

Figure 2.1. The overview of CO_2 splitting using molten salt electrolysis.

Besides these reactions above, several side reactions can be considered to happen, depending on the reaction conditions. The formation of carbon monoxide may be the most probable side reaction during this process.

$$CO_3^{2-} + 2e^- \rightarrow CO(g) + 2O^{2-} \quad (8)$$

This reaction is a partial reduction reaction of CO_2 and can be an unfavourable side reaction for maximising the yield of elemental carbon. However, since CO is also an important material in industry, some studies have focused on selectively obtaining CO gas rather than solid carbon.[27], [28]

Furthermore, metal deposition at the cathode can take place. In $CaCl_2$-NaCl molten salt, Na and Ca deposition are the possibilities.

$$Na^+ + e^- \rightarrow Na \quad (9)$$

$$Ca^{2+} + 2e^- \rightarrow Ca \quad (10)$$

The standard potentials of these reactions can be an indication of how difficult or easy to achieve each reaction. Table 2.1 shows the standard electrode potentials of the cathodic reactions with respect to the oxygen evolution reaction (Eq. 6) at 700°C. The detailed calculation will be found in Appendix C.

Table 2.1: Standard potentials for cathodic reactions at 700°C.

Cathodic reaction	Standard potential / V vs. O_2/O^{2-}
$CO_3^{2-} + 4e^- \rightarrow C + 3O^{2-}$	-1.095
$CO_3^{2-} + 2e^- \rightarrow CO(g) + 2O^{2-}$	-1.165
$Na^+ + e^- \rightarrow Na$	-1.458
$Ca^{2+} + 2e^- \rightarrow Ca$	-2.763

2.1.2 Literature review related to CO_2 electrolysis in molten salts

Studies on electro-deposition of carbon do not necessarily have a very long history. The phenomenon of deposition of carbon from carbonate molten salts was reported around the 1960s or further before.[29], [30] Despite the discoveries, this process has not been appreciated until recently. But due to the global warming and movements towards a carbon-neutral society, many studies have been reported in recent years.[17], [20], [31] In addition to this, the extensive development of carbon-based nanomaterials may also be another reason to motivate this kind of study, as the strong demands for new economical and efficient production routes have been largely increased.

In the early 2000s, deposition of carbon film from carbonate molten salts was developed. Kawamura *et al.*[32] confirmed that carbon films were formed on aluminium substrates with different morphologies and cohesiveness in a LiCl-KCl-K_2CO_3 molten salt. Massot *et al.*[33] reported the deposition of carbon film in molten LiF-NaF-Na_2CO_3. They found that the cathodic processes are completely controlled by the diffusion of carbonate ions in the melt. It was also revealed that these carbon films were basically amorphous and they did not have unique nanostructures.

On the other hand, electrolytic formation of carbon nanotubes (CNTs) in LiCl molten salt was reported by Hsu *et al*[34] in 1995. This is the first study that demonstrated the formation of carbon nanotubes in a condensed phase, but this was not CO_2 electrolysis, as the carbon source of CNTs were exfoliated graphitic sheets originating from the carbon cathode. This reaction was achieved by the intercalation of Li into the carbon cathode, where exfoliated graphitic sheets are rolled and form nanotubes.

Since CO is also an important material in industries, electrolytic CO formation from carbonate salts has also been investigated. Kaplan *et al.*[27] used Ti as the cathode material in Li_2CO_3 molten salt. Although this system had an issue that Li_2CO_3 can be decomposed into Li_2O and CO_2, the titanium cathode showed good selectivity for CO formation rather than carbon deposition reaction. Matsuura *et al.*[28] studied CO evolution in $CaCl_2$-CaO molten salt by using a stainless steel cathode and a zirconia anode. They also investigated the effect on the selectivity of the CO_2 gas, and it was shown that a high concentration of CO_2 enhanced the CO evolution rather than carbon deposition.

Electrolytic formation of carbon nanofibers (CNFs) in molten carbonate salts was reported by Ren *et al.*[35]. They achieved high controllability of carbon nanofibre products by adding metal additives and changing current density. The added metals such as Ni or Zn worked as nucleation sites and contributed to the uniformity of the products. The remarkable point of this study is that they achieved the direct conversion of CO_2 into CNFs. It was later confirmed that the carbon products originated from CO_2 gas introduced in the system, by using a $^{13}CO_2$ isotope.[36]

Encapsulation of metals in carbon materials has been strongly desired since it can enhance the performance of battery materials. Weng *et al.*[37] discovered that Ge nanoparticles can be encapsulated in carbon nanotubes (Ge@CNTs) by electrolysis in molten $CaCl_2$-NaCl-CaO with GeO_2. CO_2 gas was generated in-situ by the anodic reaction. Then, it forms ${CO_3}^{2-}$ and can be reduced to carbon, which surrounds Ge nanoparticles reduced at the cathode.

Hu *et al.*[38] found that graphene sheets can be produced from CO_2 in a $CaCl_2$-NaCl-CaO molten salt system. The key points of this process are the catalytic effect of the metal species resulting from the cathode and the microexplosion of

CO gas, which is produced simultaneously at the cathode. They also measured the diffusion coefficient of CO_3^{2-}. It was 1.68×10^{-5}[cm^2/s] at 750°C.

Fabrication of nanodiamonds by an electrolytic route was reported by Kamali *et al.*[39], [40]. This was achieved in LiCl molten salt with simultaneous injection of moisture and CO_2. Due to the intercalation of Li and H atoms into the graphite cathode, the graphite sheets are exfoliated and they cover Li_2CO_3 nanocrystals upon cooling. This carbon-Li_2CO_3 nanocomposite acts as a nanoreactor in the heating process, and it results in the formation of nanodiamonds from the carbonate.

Carbon nanospheres are also an interesting product fabricated by CO_2 electrolysis. Deng *et al.*[41] reported the formation of hollow carbon spheres from a molten LiCl-KCl-$CaCO_3$ system. Unique nanostructures including stripe patterns and wrinkles as well as nano spheres were obtained. The authors attributed the reason why these unique morphologies are obtained to the formation of micro-sized CO bubbles.

Other diverse carbon nanomaterials can also be synthesised by electro-splitting of CO_2. Liu *et al.*[42] reported the formation of carbon nano-onions in Li_2CO_3-based molten salt. Wang *et al.*[43] found a synthesis route of Carbon Nano-Scaffold (CNS), which is a three-dimensional structure made up of graphene sheets.

Although it has been shown that various carbon materials can be obtained by CO_2 elecrto-splitting in molten salts with various experimental conditions, the number of reports focusing on the reaction mechanism or the detailed cathodic behaviour is still limited.

Ito *et al.* investigated the reduction and re-oxidation process of carbonate in LiCl-KCl melt.[25] They proposed the two-step electrochemical reduction mechanism of carbonate. From chronopotentiometry, the diffusion coefficient of carbonate ion was estimated to be 1.66 ($\pm$0.05) $\times$ 10^{-5}[cm^2/s] at 450°C. The activation energy was also determined from the Arrhenius plot, which was 1.43 ($\pm$0.15)[kJ/mol].

Ge *et al.*[44] investigated the nucleation process of carbon in LiCl-Li_2CO_3 molten salt mainly with an SEM analysis after electrolysis. They employed short-term electrolysis with various conditions and revealed that the morphologies of the products vary depending on the substrates and the cell voltages.

Studies on inert anodes have also been extensively done by many research groups. Inert anodes used in CO_2 electrolysis in molten salts can be categorised as the following: metals, alloys, and oxides.[20] Each of them has advantages and drawbacks. Typically, metals and alloys are advantageous in terms of physicochemical properties such as electrical conductivity and mechanical strength. But they tend to show poorer stability, particularly in halide molten salts, and some metals such as Ir or Pt are much more expensive than oxides. Since halides are very important

electrolyte materials in molten salt chemistry and industry, development of oxide inert anodes is one of the important topics.

SnO_2 has been known to be a relatively stable material even in a highly corrosive molten salt environment. Due to the poor physical properties of SnO_2 itself, additives such as CuO and Sb_2O_3 have been used when it is utilised for electrode materials.[45] This SnO_2-based electrodes have been widely investigated and proved to be fairly inert in various molten carbonate and chloride systems.[23], [46]

Although SnO_2-based electrodes are widely accepted as a stable anode material, the conductivity and the mechanical strength are still not as good as metals. Also, it is known that a $CaSnO_3$ layer can be formed on the surface of tin oxide electrodes in CaO-containing molten salts, which drastically decreases the electrical conductivity.[47] Furthermore, $CaSnO_3$ can be reduced by alkali/alkaline earth metals and it forms soluble Sn metals, meaning that the electrode is gradually consumed.

To address these issues, in recent years, composite oxide materials, such as $CaRuO_3$[47], $CaTi_{1-x}Ru_xO_3$[48], and $TiO_2 \cdot RuO_2$[49] inert anodes have been developed. Even though the high cost of Ru is a big drawback compared to cheap SnO_2 anodes, it has been demonstrated that they show better conductivity as well as quite good stability in molten chlorides and carbonate salts.

2.2 Electrochemical measurements

2.2.1 Potential sweep methods

Potential sweep techniques are the most widely used measurement methods in electrochemistry. Owing to their availability and the great amount of information they can give us, they are frequently performed as the first choice for the study of various electrochemical systems. As the name suggests, the main idea is to control and sweep the potential of the working electrode at a certain rate. Simultaneously, the current is recorded at each potential. It enables us to visualise the change of the current as a function of potential. There are two most common techniques: Linear Sweep Voltammetry (LSV) and Cyclic Voltammetry (CV).

Linear sweep voltammetry (LSV) is a technique to sweep the potential linearly, according to the following equation.

$$E(t) = E_0 \pm \nu t \tag{11}$$

Here, *E(t)* is the potential of the working electrode, E_0 is the potential to start the sweep, ν is the scan rate, and t is time. The plus and minus signs are representing sweeps to the anodic or cathodic directions, respectively. A typical $E-t$ curve and its current response are shown in Fig 2.2.

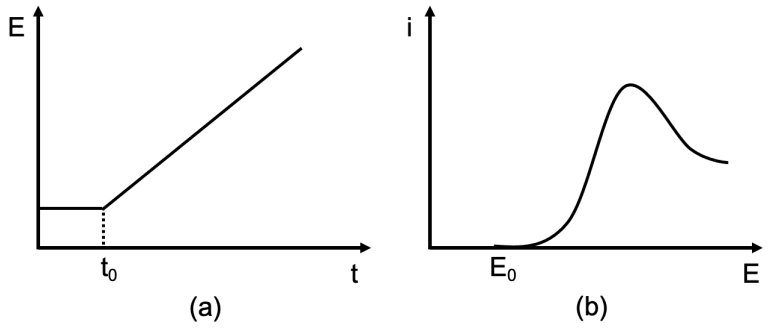

Figure 2.2. (a) Typical E-t plot during a linear sweep, (b) Typical linear voltammogram.

The information obtained from this kind of plots is quite diverse and can be used for both qualitative and quantitative analysis of the system. Some of the most important theories behind it are introduced below.

We consider a simple redox system.

$$\mathrm{Ox} + \mathrm{ne}^- = \mathrm{Red} \tag{12}$$

Ox is an oxidising agent, n is the number of electrons transferred, and Red is a reducing agent. For simplicity, we here assume that diffusion occurs in a planar geometry without any other transportation processes, and the reducing agent does not exist at the initial condition at all.

In such a simple system, the relation between the current density and the concentration at the surface of the electrode can be expressed according to Fick's first law.

$$-J_{\mathrm{Ox}}(x) = \frac{-I}{nFA} = D_{\mathrm{Ox}} \frac{\partial C_{\mathrm{Ox}}(x)}{\partial x} \tag{13}$$

$J_{\mathrm{Ox}}(x)$ is the flux of the oxidising agent, I is the current, n is the number of electrons that are exchanged, F is the Faraday constant, A is the area of the electrode, and $C_{\mathrm{Ox}}(x)$ is the concentration of the oxidising agent. If this equation is represented using the current density (i),

$$i = -nFD_{\mathrm{Ox}} \left. \frac{\partial C_{\mathrm{Ox}}(x)}{\partial x} \right|_{x=0} \tag{14}$$

When the concentration varies depending on the time, the current density also changes accordingly. So, it is convenient to know the time dependence of the current. It can be obtained from Fick's second law.

$$\frac{\partial C_{\mathrm{Ox}}(x,t)}{\partial t} = D_{\mathrm{Ox}} \frac{\partial^2 C_{\mathrm{Ox}}(x,t)}{\partial x^2} \tag{15}$$

To solve this partial differential equation, the following conditions are applied:

$$\text{(i) All x and t} = 0 \ ; \ C_{\mathrm{Ox}}(x,0) = C^{*}_{\mathrm{Ox}}, \ C_{\mathrm{Red}}(x,0) = 0 \tag{16}$$

$$\text{(ii) x} \rightarrow \infty \text{ and all t} \ ; \ C_{\mathrm{Ox}}(x,t) = C^{*}_{\mathrm{Ox}}, \ C_{\mathrm{Red}}(x,0) = 0 \tag{17}$$

$$\text{(iii) x} = 0 \text{ and t} > 0 \ ; \ J_{\mathrm{Ox}} = -J_{\mathrm{Red}}$$

i.e.,

$$D_{\mathrm{Ox}}\frac{\partial C_{\mathrm{Ox}}(x,t)}{\partial x} = -D_{\mathrm{Red}}\frac{\partial C_{\mathrm{Red}}(x,t)}{\partial x} \tag{18}$$

For a "reversible" system, where the rate of electron transfer is much faster than mass transport, one more condition is considered. There, the relationship between the potential and concentration of species can be expressed by using Nernst equation (Eq.19). Due to this, reversible systems can also be referred to as "Nernstian".

$$E = E^{\circ'} + \frac{RT}{nF}\ln\frac{C_{\mathrm{Ox}}(0,t)}{C_{\mathrm{Red}}(0,t)} \tag{19}$$

$E^{\circ'}$ is the formal potential, R is the gas constant, T is the absolute temperature, and C_i is the concentration of species i. Eq.19 can be rewritten as:

$$\frac{C_{\mathrm{Ox}}(0,t)}{C_{\mathrm{Red}}(0,t)} = \exp\Big\{\frac{nF}{RT}(E - E^{\circ'})\Big\} \tag{20}$$

If Eq.11 is inserted with a minus sign as we are considering a cathodic process,

$$\frac{C_{\mathrm{Ox}}(0,t)}{C_{\mathrm{Red}}(0,t)} = \exp\Big\{\frac{nF}{RT}(E_0 - \nu t - E^{\circ'})\Big\} \tag{21}$$

It is not easy to perform a Laplace transform to this equation due to the existence of time dependence. However, some analytical or numerical methods have been considered regarding this problem.[50], [51] The current at a certain time and scan rate can be expressed as:

$$I = -nFAC^{*}_{\mathrm{Ox}}\sqrt{\pi D_{\mathrm{Ox}}\sigma}\ \chi(\sigma t) \tag{22}$$

Here, C^{*}_{Ox} is the bulk concentration, D_{Ox} is the diffusion coefficient, σ is $(nF/RT)\nu$, and χ is a number that can be numerically obtained from Eq. 23. From Eq. 22, it can be seen that the current is proportional to the bulk concentration of Ox and $(\text{scanrate})^{1/2}$.

$$\int_0^{\sigma t}\frac{\chi(z)}{\sqrt{(}\sigma t - z)}dz = \frac{1}{1 + \xi\theta S(\sigma t)} \tag{23}$$

where ξ is $\sqrt{\frac{D_{\mathrm{Ox}}}{D_{\mathrm{Red}}}}$ and $S(\sigma t)$ is $e^{-\sigma^2 t}$. The values of $\pi^{1/2}\chi(\sigma t)$ are tabulated and available.[51] From the table, one can find that $\chi(\sigma t)$ reaches the maximum at some point, which is 0.4463. From the value and Eq. 22, the peak current I_p is

$$I_p = -0.4463\sqrt{\frac{n^3F^3}{RT}}AC^*_{\mathrm{Ox}}\sqrt{D_{\mathrm{Ox}}\nu} \tag{24}$$

This equation is known as "Randles-Ševčík equation". Following this relation, if we plot I_p against $\nu^{1/2}$, a straight line can be obtained. This makes it possible for us to calculate the diffusion coefficient (if the bulk concentration is known) or the bulk concentration (if the diffusion coefficient is known).

As for the potential giving us the peak current, E_p can be expressed as the following:

$$E_p = E_{1/2} - 1.109\frac{RT}{nF} \tag{25}$$

$E_{1/2}$ is called the half wave potential, which is defined by

$$E_{1/2} = E^{0'} - \frac{RT}{nF}\ln\sqrt{\frac{D_{\mathrm{Ox}}}{D_{\mathrm{Red}}}} \tag{26}$$

Unfortunately, the peak of voltammograms can often be broad and it is not easy to determine the exact location of the peak potential. In such cases, the potential that gives us $I_p/2$ is convenient. It is called the half-peak potential ($E_{p/2}$).

$$E_{p/2} = E_{1/2} + 1.09\frac{RT}{nF} \tag{27}$$

The difference between E_p and $E_{p/2}$ can be used to diagnose the reversibility of the redox system.

$$|E_p - E_{p/2}| = 2.20\frac{RT}{nF} \tag{28}$$

So far, the reduced species has been assumed to be completely soluble. However, if the reduction process involves in deposition of insoluble species, like metal deposition, different approaches are needed. This kind of problem was firstly solved by Berzins and Delahay.[52] When the product is insoluble, the current is expressed as follows:

$$I = -2nFAC^*_{\mathrm{Ox}}\sqrt{\frac{D\sigma}{\pi}}\Phi(\sqrt{\sigma t}) \tag{29}$$

This equation corresponds to Eq. 23 when insoluble species are involved. Here, $\Phi(\alpha)$ is a function called the Dawson function, which is represented as

$$\Phi(\alpha) = \exp(-\alpha^2)\int_0^\alpha \exp(z^2)dz \tag{30}$$

$\Phi(\alpha)$ shows a maximum value, 0.5410, at $z = 0.9241$. The corresponding equation to the Randles-Ševčík equation in this case is

$$I_p = -0.6105\sqrt{\frac{n^3F^3}{RT}}AC^*_{\mathrm{Ox}}\sqrt{D_{\mathrm{Ox}}\nu} \tag{31}$$

The peak potential E_p is the following. Here, E_{rev} is the reversible potential.

$$E_p = E_{\mathrm{rev}} - 0.8540\frac{RT}{nF} \tag{32}$$

When the direction of the sweep is changed at a certain time ($t = \lambda$) (or a certain potential E_λ), it is called cyclic voltammetry (CV).

$$(0 < t \leq \lambda);\ E = E_0 - \nu t \tag{33}$$

$$(t > \lambda);\ E = E_0 - 2\nu\lambda + \nu t \tag{34}$$

A typical $E - t$ plot and $i - E$ curve are presented in Figure 2.3. This technique makes it possible to study both of the processes of reduction and re-oxidation (and/or the opposite) in one potential sweep, and this is by far the most common choice as the first diagnosis of electrochemical systems.

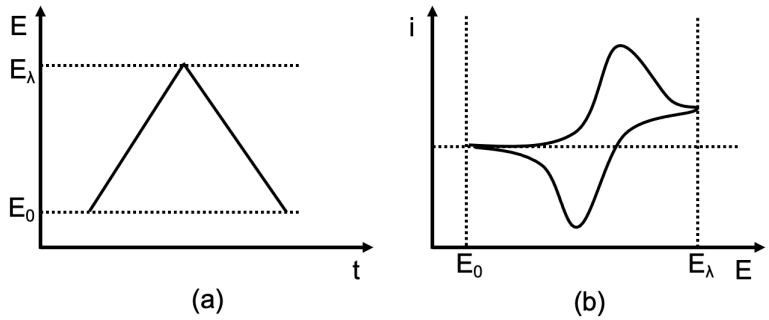

Figure 2.3. (a) Typical E-t plot during a triangular sweep, (b) A typical cyclic voltammogram.

2.2.2 Chronoamperometry

Chronoamperometry is a technique to investigate the current transient by applying a constant potential to the working electrode step by step. That is why this kind of measurements can also be referred to as "potential step" methods.

From Fick's second law,

$$\frac{\partial C_{\mathrm{Ox}}(x,t)}{\partial t} = D_{\mathrm{Ox}}\frac{\partial^2 C_{\mathrm{Ox}}(x,t)}{\partial x^2} \tag{35}$$

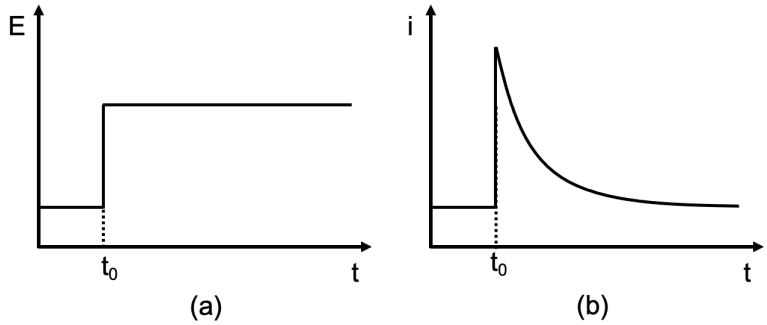

Figure 2.4. (a) A typical E-t plot during a potentials step experiment, (b) A typical i-t plot.

The following boundary conditions are applied to solve this partial differential equation.

$$\text{(i) All x and t} = 0 \; ; C_{\mathrm{Ox}}(x,0) = C^*_{\mathrm{Ox}} \tag{36}$$

$$\text{(ii) x} \rightarrow \infty \text{ and all t} \; ; C_{\mathrm{Ox}}(x,t) = C^*_{\mathrm{Ox}} \tag{37}$$

$$\text{(iii) x} = 0 \text{ and t} > 0 \; ; C_{\mathrm{Ox}}(0,t) = 0 \tag{38}$$

By Laplace transforming the Fick's second law,

$$s\overline{C_{\mathrm{Ox}}}(x,s) - C^*_{\mathrm{Ox}} = D_{\mathrm{Ox}} \frac{d^2\overline{C_{\mathrm{Ox}}}(x,s)}{dx^2} \tag{39}$$

$$\frac{d^2}{dx^2}\left\{\overline{C_{\mathrm{Ox}}}(x,s) - \frac{C^*_{\mathrm{Ox}}}{s}\right\} - \frac{s}{D_{\mathrm{Ox}}}\left\{\overline{C_{\mathrm{Ox}}}(x,s) - \frac{C^*_{\mathrm{Ox}}}{s}\right\} = 0 \tag{40}$$

The equation (40) can be regarded as a simple ordinary differential equation and can be easily solved. The general solution is

$$\overline{C_{\mathrm{Ox}}}(x,s) = \frac{C^*_{\mathrm{Ox}}}{s} + A\exp\sqrt{\frac{s}{D_{\mathrm{Ox}}}} + B\exp\left(-\sqrt{\frac{s}{D_{\mathrm{Ox}}}}\right) \tag{41}$$

By applying the boundary condition (ii), one can tell that the constant A must be zero. Also, from the condition (iii), the constant B can be obtained, which is $-\frac{C^*_{\mathrm{Ox}}}{s}$. Therefore,

$$\overline{C_{\mathrm{Ox}}}(x,s) = \frac{C^*_{\mathrm{Ox}}}{s} - \frac{C^*_{\mathrm{Ox}}}{s}\exp\left(\sqrt{\frac{s}{D_{\mathrm{Ox}}}}x\right) \tag{42}$$

Combining with Fick's first law and inverse Laplace transforming, as a result,

$$\overline{I}(s) = -nFAC^*_{\mathrm{Ox}}\sqrt{\frac{D_{\mathrm{Ox}}}{s}} \tag{43}$$

$$I_{\mathrm{lim}}(t) = -nFAC^*_{\mathrm{Ox}}\sqrt{\frac{D_{\mathrm{Ox}}}{\pi t}} \tag{44}$$

The final equation is known as "Cottrell equation". If the potential is sufficiently negative (in the case of reduction) to meet the condition (iii), the limiting current can be obtained, where the current transient is controlled solely by the diffusion. The limiting current is plotted as a function of $t^{-1/2}$ and the diffusion coefficient can be obtained from the slope of the straight line.

Chronoamperometry is also a powerful tool to investigate the nucleation processes of metals. It has been extensively studied in various electrochemical systems, and it is known that it is useful to determine the induction time, the rate constant, and the number of nuclei.[53] Figure 2.5 shows a typical $i - t$ plot when the kinetics of the phase formation is governed by the nucleation process at the initial stage of the current transient.

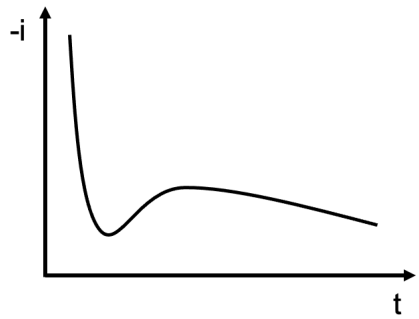

Figure 2.5. Typical i-t plot for the nucleation of metal on a foreign substrate.

First, the charging current of the electric double layer can be observed. After this, the formation of small nuclei takes place and the current decreases rapidly. The nuclei continue incorporating the reactant in the vicinity. As the growth proceeds, the active surface area of the electrode increases and the current is also increased accordingly. When the diffusion zone of each nucleus overlaps, the supply of the reactant is limited and the further growth is suppressed. This is the reason why the peak current appears in Figure 2.5. After the peak, the current is controlled by linear diffusion and decreases according to Cottrell equation.

3 Experimental

3.1 Chemicals and apparatus

3.1.1 Electrolytes

During this project, $CaCl_2$-NaCl-CaO (or $CaCO_3$) molten salt systems were used as an electrolyte. The molar ratio of $CaCl_2$ and NaCl was fixed to 0.80 : 0.20. All the chemicals used are summarised in Table 3.1.

Table 3.1: Chemicals used in the experiments.

Formula	Purity/%	Company	Product number
$CaCl_2 \cdot 2\,H_2O$	≥99.9	Sigma-Aldrich	223506
NaCl	≥99.5	Sigma-Aldrich	1.06404
CaO	≥99.9	Sigma-Aldrich	208159
$CaCO_3$	≥99.9	Sigma-Aldrich	239216
AgCl	≥99.998	Sigma-Aldrich	449571

3.1.2 Electrodes

For the working electrodes, four different materials were employed: W, Mo, graphite, and glassy carbon. W and Mo are known to be inert in various molten salt systems at elevated temperatures and they have been extensively used for studying the cathodic behaviours of various metals. Graphite and glassy carbon are also typical electrode materials owing to the stability at high temperatures under inert atmosphere and in molten salts. W and Mo were also used as a cathode for electroytic studies.

As a counter electrode, graphite crucible (Schunk Tokai) and an SnO_2 rod (STANNEX ELR, Glassworks Hounsell Ltd.) were used. The composition of STANNEX ELR is as follows: SnO_2: 98.55%, Sb_2O_3: 1%, and CuO: 0.45%. Sb_2O_3 is playing a role to improve the electrical conductivity and CuO is a sintering aid.[45] They were also tested as an anode for electrolysis.

As the reference electrode, a handmade Ag/AgCl reference electrode with a mullite membrane or a W wire quasi-reference electrode was used.

3.1.3 Electrochemical cell

3.1.4 Furnace and gas flow system

All the experiments were carried out in a muffle electric furnace (L100-V) in K2-407 (Fig. 3.1). The temperature was monitored with a type-K thermocouple placed at the centre of the furnace. The surface of the furnace was cooled by circulated water.

This feature makes it possible to prevent the surface from becoming too hot, which enables us to avoid damaging items around the furnace, and more importantly, to protect ourselves. The water flow was checked by a flow monitor (Flowswitch DW-K, HENKE SASS WOLF), and the main power of the furnace is cut off when the monitor cannot detect water flow.

An alumina tube (length = 70 cm, $\phi_{\text{inner}} = 10$ cm, $\phi_{\text{outer}} = 11.5$ cm) was placed in the furnace as a chamber wall. The top and bottom ends were sealed with metal lids and O-rings made of rubber so as to make the system gas-tight. An inert gas (Ar) was introduced from the bottom, which was supplied from the central gas system. The Ar flow was controlled with a variable area flow meter (V-100, Vögtlin Instruments GmbH). When a simulated exhaust containing CO_2 was introduced from the top, the Ar gas inlet at the bottom was closed. The gas outlet was on the top of the furnace for both cases, and it was connected to two gas-washing bottles: the first one was empty and the other was filled with some oil, to prevent the oil from entering the system in case of backflow, and to visually monitor the gas flow, respectively. The outlet gas was finally sent to the central ventilation system.

For CO_2 gas flow, a gas flow system with multiple valves and mass flow controllers (EL-Flow Select, Bronkhorst) was used.(Fig. 3.2) Since this gas flow system was originally designed and used for CH_4, Ar, and H_2, the mass flow controllers had been also calibrated accordingly. Therefore, the output signals of the flow controllers were converted with the gas conversion factors. N_2 gas was supplied from the central gas system and was used to dilute CO_2 gas to simulate the exhaust from industrial processes. A CO_2 gas cylinder was purchased from Linde gas AS (HIQ CARBON DIOXIDE 5.3 10 L, Purity: $\geq$ 99.99%). The gas flow rate was monitored and controlled with LabVIEW 8.5 (National Instruments). CO_2 or CO_2-N_2 mixture was introduced from the top lid. For a bubbler, an alumina tube was immersed in the melt.

3.2 Procedures

3.2.1 Preparation of salts

In order to remove water contained in salts, all the salts were heated in an oven before the series of experiments. $CaCl_2 \cdot 2\,H_2O$ was dried at 200°C at least for 24 hours to remove the crystal water molecules. A typical water removal rate calculated from the weight loss was over 99.5%. NaCl and $CaCO_3$ were heated at 110°C at least for 24 hours to get rid of the adsorbed moisture. CaO was obtained by calcining CaO or $CaCO_3$ at 1000°C for 2 hours, as CaO easily absorbs CO_2 in the air and the real composition becomes unknown.

3.2.2 Preparation of electrodes

All the detailed dimensions of electrodes will be found in Appendix E. Here, only the procedures to construct them will be described.

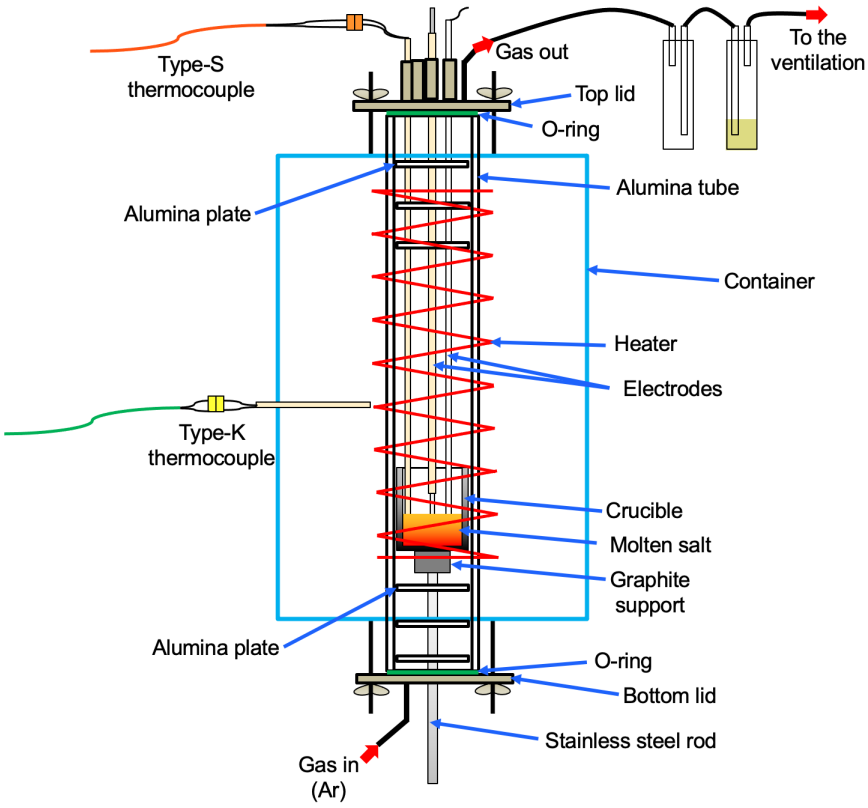

Figure 3.1. Cross section of the electric furnace (L100-V).

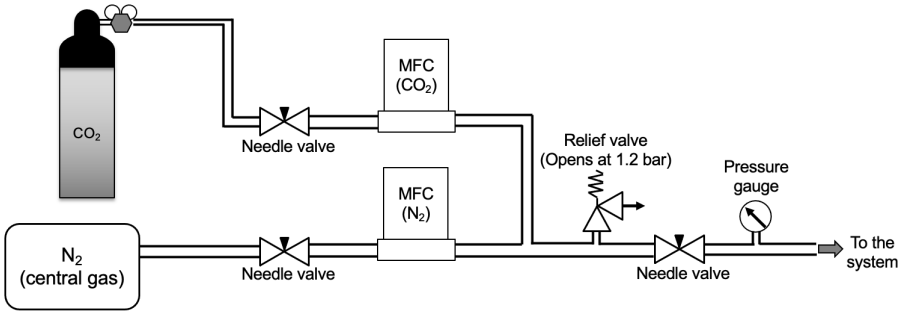

Figure 3.2. Schematic of the gas flow system used for the series of experiments.

W and Mo wire electrodes were fabricated by the following manner: first, a metal wire was washed with water and well polished with SiC abrasive paper. The wire was inserted into an alumina tube (Alsint, Morgan Technical Ceramics) for protection and insulation, and it was fixed to the alumina tube at the top by using silicone paste (LOCTITE SI 5940).

To construct graphite electrodes, graphite rods were machined by using a drill to make screw holes. A stainless steel rod with threads were inserted into the rod to establish an electrical connection. The steel rod was covered with an alumina tube as with the W and Mo wire electrodes and fixed to the alumina tube with silicone paste.

As for glassy carbon electrodes, a glassy carbon rod was first inserted into a graphite rod with a hole, since it is difficult to machine glassy carbon itself. On the other side of the graphite rod, a screw hole was made to be able to attach a steel rod and make an electrical connection. The steel rod was protected by an alumina tube likewise.

Graphite crucibles were purchased and used as the counter electrode without any alteration. SnO_2 counter electrodes required some special tricks to fabricate them. The detailed procedures are described in Appendix F.

Ag/AgCl reference electrodes were made by the following procedures: a mullite tube (Pythagoras, Morgan Technical Ceramics) was used as a membrane. There, a silver wire was inserted. In order to make the silver wire as durable as possible in the molten salt, the wire was wound and a coil was made. Mixture of salts with the same composition as the melt was added from the top of the tube, in addition to a small amount of AgCl (5 mol%). The top of the mullite tube was then sealed with silicone paste. The salt can be molten in the furnace during the experiment, and an AgCl layer can be formed on the surface of the silver wire. The silver wire was occasionally replaced during the experiments when the silver wire was corroded. However, since the lifetime of silver wires was not very long, W wire quasi reference electrodes were also occasionally used. They were fabricated in the same manner as W wire working electrodes.

3.2.3 Construction of the cell

Before the preparation of the cell, a graphite crucible was dried in an oven at 110 °C to remove moisture. Salts were also dried as described before. The dried salts were weighed and mixed well before putting them in the crucible. The crucible filled with the salts was carefully placed on the graphite support in the furnace.

Electrodes, a thermocouple, and a bubbler(or a feeding tube) were also dried in

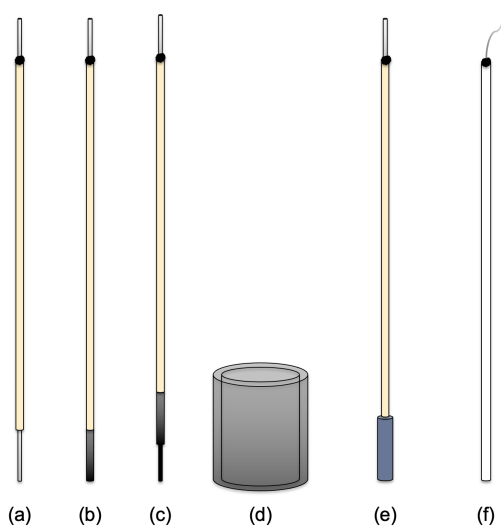

Figure 3.3. Illustration of electrodes used for the experiments: (a) W or Mo wire electrode, (b) Graphite electrode, (c) Glassy carbon electrode, (d) Graphite crucible (counter electrode), (e) SnO_2 electrode, and (f) Ag/AgCl reference electrode.

an oven at 110 °C before use. They were fixed to the top lid by using rubber corks. Some silicone grease (Dow Corning® high-vacuum silicone grease) was put between the rubber corks and alumina tubes. The purpose of this is to improve the sealing ability and lubricate the tubes, making it easier to shift the heights of them during experiments. Next, the top lid was fixed on the top of the furnace. The connection part was sealed with an O-ring made of rubber. Silicone grease was applied to this part as well.

After the lid was fixed, the gas inlet was connected to the gas system. An inert gas (Ar) was introduced and the atmosphere inside the furnace was replaced. Then, the furnace was pre-heated at 300°C for at least 1 hour. After pre-heating, the temperature was increased up to 800°C.

3.2.4 Electrochemical measurements

Electrochemical measurements were performed with a three-electrode configuration. IVIUM-n-STAT (IVIUM TECHNOLOGIES) was employed as a potentiostat.

When CO_2 gas (pure or diluted) was used, it was continuously bubbled before electrochemical measurements at least for 30 minutes at 150 mL/min. During voltammetry, the bubbler was pulled up so that the disturbance by the bubbling can be mitigated. After each voltammetry, the bubbler was again inserted into the

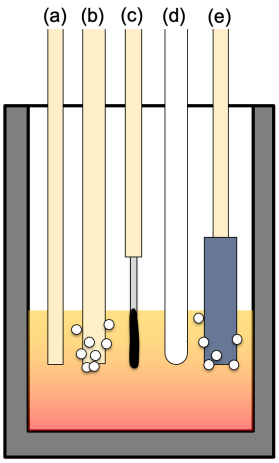

Figure 3.4. Typical configuration of the electrochemical cell: (a) Thermocouple, (b) Bubbler, (c) Working electrode, (d) Reference electrode, and (e) Counter electrode.

melt at least 5 minutes for giving convection and resupplying the reactant to the melt.

Calcium oxide or calcium carbonate was added either initially or later. When adding the reagent later, an Alsint tube was inserted from the top lid and used as a guide tube to the molten salt bath. After the addition of the salt, the molten salt mixture was left at least for 2 hours to ensure that it is completely dissolved.

3.2.5 Collecting the product and characterisation

After electrochemical measurements, the furnace was cooled down to room temperature. Then, the electrodes were retrieved. The cathode was washed with water and hydrochloric acid to remove the salts. The suspension containing product was sonicated with an ultrasonic bath and collected by suction filtration, where a membrane filter(Omnipore Membrane Filter, JVWP04700) was employed. The obtained product was then dried in air and separated from the filter.

The product was then characterised with an SEM-EDS (Zeiss SUPRA 55 FESEM) and a powder XRD diffractometer (Bruker D8 ADVANCE).

4 Results and discussions

4.1 Behaviour of carbonate ions in $CaCl_2$-based molten salts

4.1.1 Voltammetry in $CaCl_2$-based molten salts containing carbonate

First, the cathodic behaviour of carbonate ions was investigated in the $CaCl_2$-NaCl (80:20 (mol%)) molten salt system by potential sweep methods. Here, four different kinds of working electrodes were employed: glassy carbon, graphite, tungsten, and molybdenum. Unless otherwise specified, graphite was used as a counter electrode.

Figure 4.1 shows typical cyclic voltammograms on a glassy carbon working electrode with and without $CaCO_3$. In chloride molten salt without carbonate, two different cathodic peaks were observed.(Fig.4.1a) For both peaks, the corresponding anodic peaks were recorded during the back sweeps, but the peak sizes were much smaller than those of the cathodic peaks. Considering the salt composition, the peak C2 can be identified as the deposition of Ca and/or Na, as the standard potentials of Ca and Na deposition are quite close values, when the anodic reaction is chlorine evolution. (See Appendix C.) The reason why the backward oxidation peak was small would be due to the dissolution of alkali/alkaline earth metals into the $CaCl_2$-NaCl molten salt, which is known to have a high capability of dissolving various metals.[54] The peaks C1 and A1 may be attributed to the intercalation of sodium atoms into the glassy carbon and its backward process .[55]

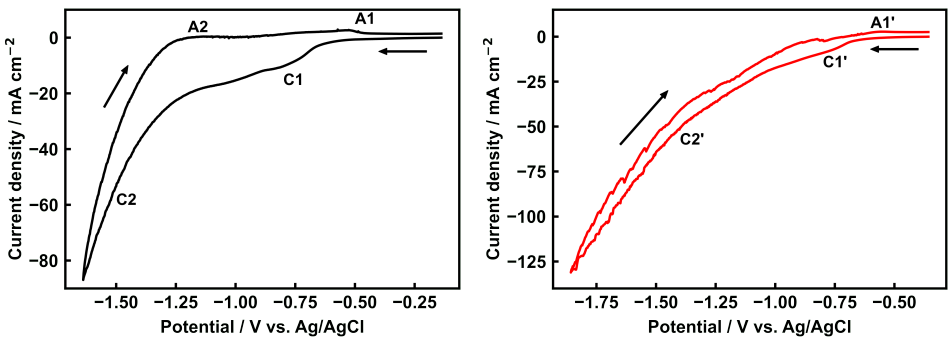

Figure 4.1. Cyclic voltammograms on a glassy carbon electrode in $CaCl_2$-NaCl (80 mol% : 20 mol%) molten salt at 800°C. (a)Without $CaCO_3$ and (b)With 0.5 mol% $CaCO_3$. Scan rate: 500 mV/s. Atmosphere: Ar.

On the other hand, after adding 0.5 mol% of $CaCO_3$, the shape of the voltammogram was drastically changed. While the first pair of peaks were still visible, the second cathodic peak was no longer the same shape and the corresponding oxidation peak was not clearly observable. The onset of the large cathodic current was

also shifted more positively. According to the standard electrode potential in Table 2.1, the carbon deposition reaction can happen at a less negative potential than Ca or Na deposition. Also, the noisier profile of the curve can indicate the deposition of some different species other than Ca or Na. Therefore, it was suggested that the peak C2' can be the carbon deposition reaction ($CO_3{}^{2-} + 4e^- = C + 3O^{2-}$).

Cyclic voltammograms using a graphite working electrode are shown in Figure 4.2. The current-potential curve showed a line-crossing around -1.7 V(vs. Ag/AgCl) and the cathodic current was larger during the backward sweep than that during the forward sweep. It indicates the increase of the active surface area of the electrode during the cathodic sweep, which can be attributed to the deposition of carbon. This kind of loop-shaped hysteresis was also sometimes seen when other electrode materials were applied, depending on the vertex and the scan rate.

The anodic peak around -0.35 V (vs.Ag/AgCl) can be considered to be the corresponding oxidation peak of the carbon deposition reaction. It was observed that the size of the oxidation peak was much smaller than the corresponding cathodic peak. Similar behaviour was reported by Ijije *et al.*[56] in Li_2CO_3-K_2CO_3 molten salt. They attributed the reason of the smaller oxidation peak to the competing CO formation and the loss of carbon products from the electrode surface. They also compared the ratio of the anodic and cathodic charges (Q^+/Q^-) by changing various experimental conditions. The typical values were around 0.5-0.6. Although it is difficult to determine (Q^+/Q^-) in the present system due to the back ground current, the ratio could be similarly small and it can be ascribed to the same reasons.

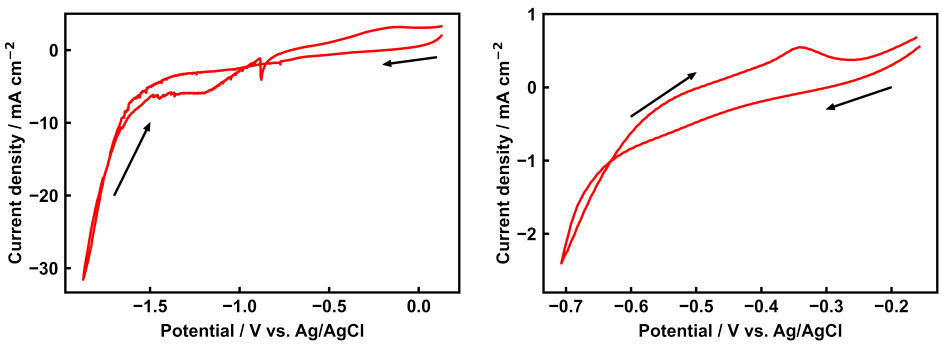

Figure 4.2. Cyclic voltammograms on a graphite electrode in molten $CaCl_2$-NaCl (80 mol% : 20 mol% + 0.5 mol%) at 800°C. (a)Wide range and (b)Narrow range. Scan rate: 500 mV/s. Atmosphere: Ar.

The cathodic behaviour in $CaCl_2$-NaCl-$CaCO_3$ molten salt on metal electrodes was also investigated. Figure 4.3 shows voltammograms using a W working electrode

with and without $CaCO_3$. When carbonate was present, two distinctive cathodic peaks were obtained. Note that the concentration of carbonate was 10 times lower than the previous voltammograms using the glassy carbon or graphite electrode. The purpose of this is to get clearer peaks and make it easy to distinguish them.

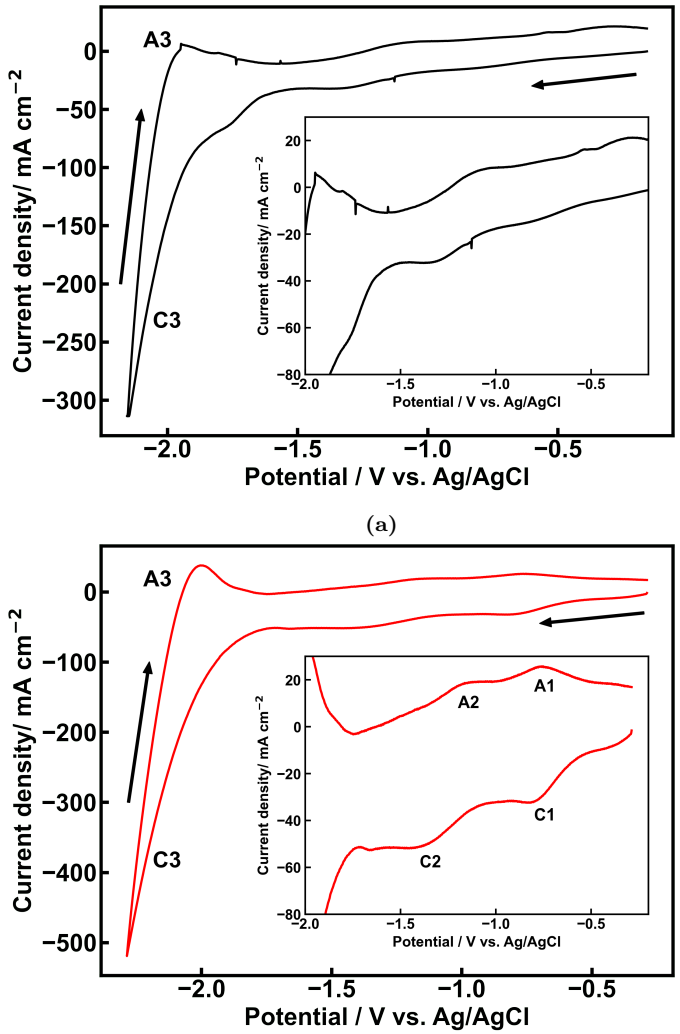

Figure 4.3. Cyclic voltammograms on a tungsten electrode in molten $CaCl_2$-NaCl (80 mol% : 20 mol%) at 800°C. (a)Without $CaCO_3$ and (b)With 0.05 mol% $CaCO_3$. Scan rate: 500 mV/s. Atmosphere: Ar.

A molybdenum wire electrode was also employed as the working electrode. Al-

most identical profiles as the tungsten electrode were obtained. That is, a two-step reduction of carbonate can be considered on molybdenum either. A typical voltammogram will be found in Appendix A.

By changing the potential limit of the sweeps, the corresponding anodic peaks were identified.(Figure 4.4) The reverse reaction of the cathodic peak C1 (around -0.75 V vs. Ag/AgCl) can be the anodic peak A1 (around -0.70 V vs. Ag/AgCl), and as for the peak C2 (around -1.40 V vs. Ag/AgCl), the peak A2 (around -1.15 V vs. Ag/AgCl) was the corresponding one.

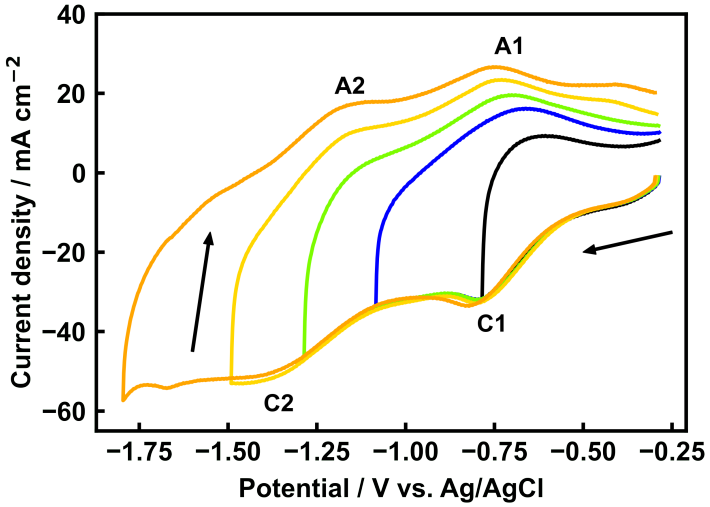

Figure 4.4. Cyclic voltammograms on a tungsten electrode in molten $CaCl_2$-NaCl-$CaCO_3$ (80 mol% : 20 mol% + 0.5 mol%) with various vertexes. Scan rate: 500 mV/s. Atmosphere: Ar.

Also, various scan rates were attempted to see the effect on the profiles.(Figure 4.5) Slight negative peak shifts were observed as the scan rate was increased. This may suggest the irreversible properties of the reactions, but the effect of the IR drop also cannot be ruled out. Even the lower concentrations of carbonate than previous voltammetries, the shape of the peaks was still vague. In addition to this, the locations of two cathodic peaks were too close to each other and it was difficult to subtract the background current. Therefore, any analysis related to the peak current and the scan rate was not carried out here.

Hu *et al.*[57] investigated the cathodic behaviour of CO_3^{2-} in a molten $CaCl_2$-$CaCO_3$ system. They also observed two different cathodic peaks during cyclic voltammetry using a W wire working electrode, which were attributed to the reduction processes of carbonate. They estimated the number of electrons that were

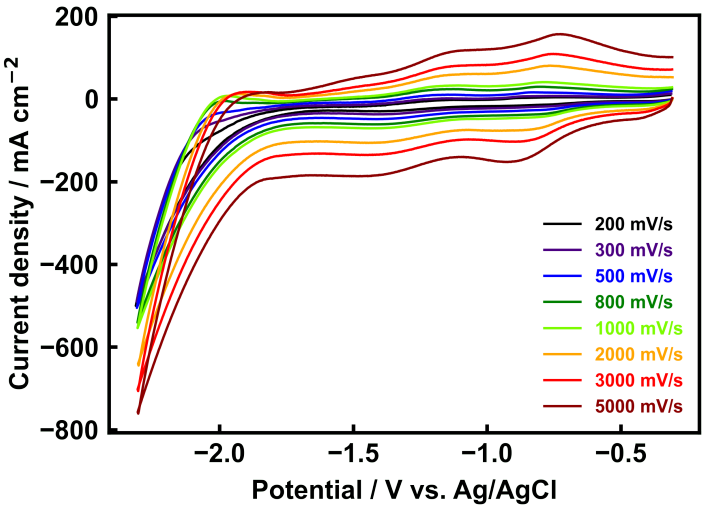

Figure 4.5. Cyclic voltammograms on a tungsten electrode in molten $CaCl_2$-NaCl-$CaCO_3$ (80 mol% - 20 mol% + 0.1 mol%) with various scan rates. Atmosphere: Ar.

exchanged at each peak by using square wave voltammetry. As a result, it was suggested that two electrons were related to each peak's reaction. They concluded that the reactions at each cathodic peak can be considered as follows:

For the peak C1,

$$CO_3^{2-} + 2e^- \rightarrow CO_2^{2-} + O^{2-} \tag{45}$$

and/or

$$CO_3^{2-} + 2e^- \rightarrow CO(g) + 2O^{2-} \tag{46}$$

For the peak C2,

$$CO_2^{2-} + 2e^- \rightarrow C + 2O^{2-} \tag{47}$$

In the present system, the corresponding oxidation peak for the first cathodic peak was clearly visible even at low scan rates. It indicates that the reduced species remained near the electrode without escaping. Therefore, the peak C1 was not a gas evolution reaction and it can be attributed to the reaction (45), and the peak C2 can be the reaction (47).

In order to ensure that the reaction was taking place according to the hypothesis above, potentiostatic electrolyses at two different cathodic peaks were carried out. Each electrolysis was performed for 2 hours at -0.97 V and -1.46 V (vs. Ag/AgCl). Figure 4.6 shows the photographs of the W cathode after each electrolysis. At peak

C1, no products were confirmed on the surface of the electrode. A shiny surface was still partly observed. In contrast, at peak C2, a small amount of black deposition was confirmed. Thus, it was confirmed that the peak C2 is the cathodic peak for carbon deposition by the reaction (47).

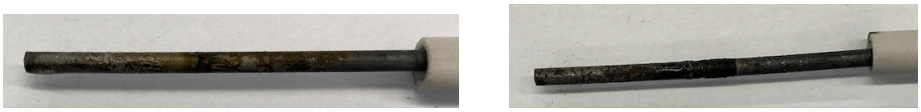

(a) **(b)**

Figure 4.6. Photographs of a tungsten electrode after 2 hours electrolysis at peak C1(a) and peak C2(b) in molten $CaCl_2$-NaCl-$CaCO_3$ (80 mol%:20 mol% + 0.1 mol%). Atmosphere: Ar.

Finally, a prolonged electrolysis around the cathodic peak C2 was performed. The potential of the cathode was kept at -1.15 V with respect to OCP (-1.61 V (vs. Ag/AgCl)) for 16 hours.

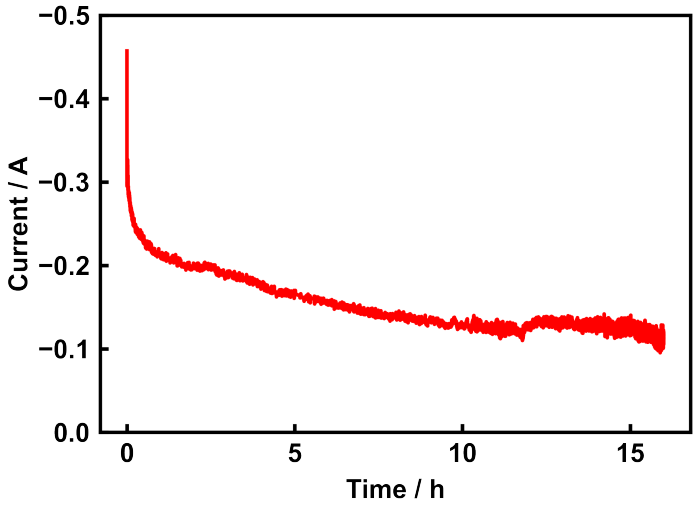

Figure 4.7. Potentiostatic electrolysis using a W cathode and a graphite anode in molten $CaCl_2$-NaCl-$CaCO_3$ (80 mol%:20 mol% + 1 mol%). Atmosphere: Ar.

The current steadily decreased as the time passed. This can be ascribed to the decreased concentration of carbonate ions in the melt. Figure 4.8 shows the photographs of the W electrode before and after electrolysis. Carbon deposition on the surface of the cathode was confirmed. After washing and collecting the carbon powder, the yield was 6.4 % of the theoretical yield. One of the reasons that decreased the yield can be simultaneous CO formation on the cathode. As it was

shown in Chapter 2, the standard potentials for carbon deposition and CO formation are quite close values at high temperatures. Gas analysis of the flue gas will be needed to confirm this in further work. Another reason for the low yield is the loss from the cathode surface due to the low cohesiveness of the carbon product. After the reaction, a significant amount of carbon powder was found in the crucible.(Appendix A., Figure A.2) So, it is considered that the carbon product fell from the surface after it was deposited on the cathode. CO production may also have promoted the detachment of the product due to the bubble formation.

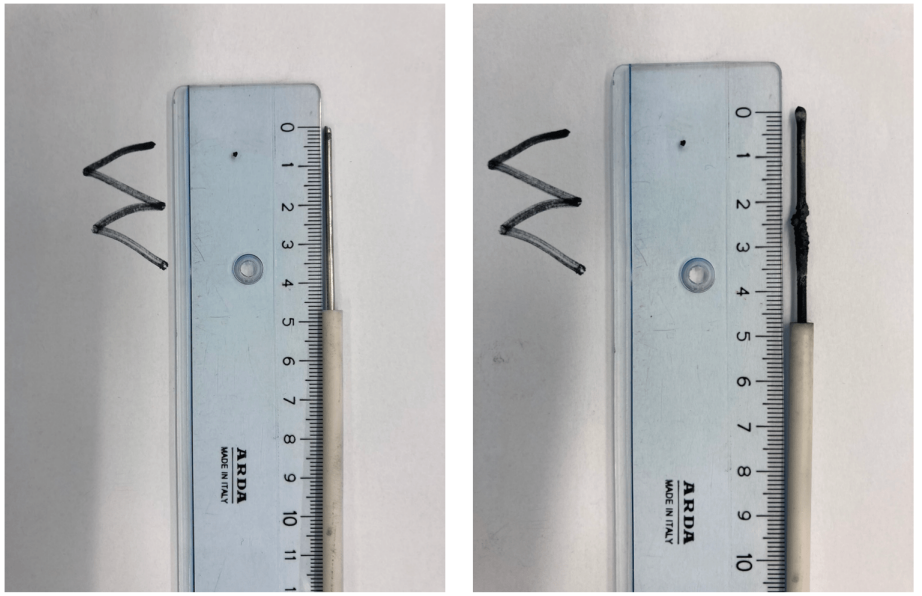

Figure 4.8. Photographs of a W electrode before (left) and after (right) electrolysis in molten $CaCl_2$-NaCl-$CaCO_3$ (80 mol%:20 mol% + 1 mol%).

Although the product was collected and the yield was calculated, it is worth mentioning that the value is not very reliable. This is one of the limitations of the series of experiments. The main reason is that the amount of collected product can be largely affected by the loss from the surface. Although considerable attention was paid when the electrode was pulled up out of the melt, the vibration and shock can promote detaching the product. So, the amount of loss cannot be always the same and it can highly depend on the case. Therefore, the value of the yield would not be reproducible. This is also the case for all the results that are presented in the later sections in this thesis.

The collected product was observed by an SEM. The size of the particles are typically under several dozens μm. The surface of the most of the product was covered with very fine fibre-like structures.(Figure 4.9)

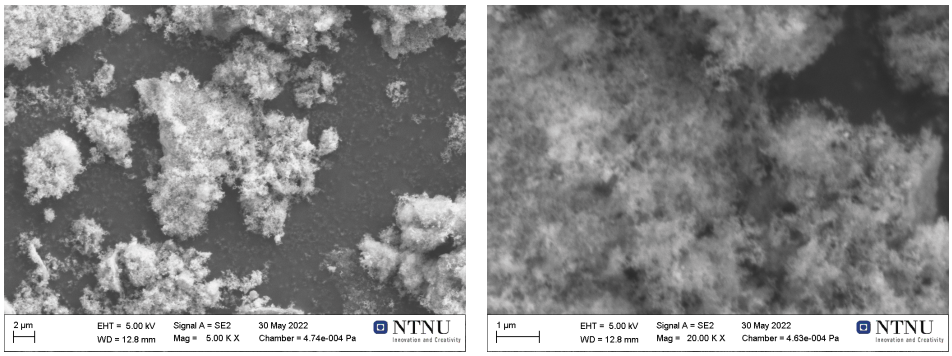

(a) **(b)**

Figure 4.9. SEM images of the carbon product obtained from potentiostatic electrolysis in molten $CaCl_2$-NaCl-$CaCO_3$ (80 mol%:20 mol% + 1 mol%) using W cathode and graphite anode. (a) Typical image of the sample and (b) Magnified image of (a).

4.1.2 Nucleation process of carbon

In order to observe the nucleation process of carbon, a potential step technique was employed. The short-term potentiostatic current transients are shown in Figure 4.10. The i-t curves did not exhibit any maximum current and the decay was simply proportional to $t^{-1/2}$. For shorter or longer time scales, any peak was not observed either.

A similar behaviour was reported by Castrillejo *et al.*[58] in Mg deposition on a tungsten electrode in molten $CaCl_2$-NaCl. They did not observe any nucleation phenomena either from voltammetry or current transient methods.

In contrast, Massot *et al.*[59] observed the nucleation of carbon in molten LiF-NaF-Na_2CO_3 system. They clearly obtained current peaks in chronoamperograms. The reason for the different behaviour from our system is likely to be due to the choice of the cathode material. In their study, a gold electrode was employed as a cathode. There are some studies reporting that carbon deposition on gold was not observed even under conditions where carbon was obtained by using other electrode materials.[60] It suggests that the surface of gold would not be very suitable for carbon to be deposited. Thus, it is reasonable that the deposition of carbon was governed by the nucleation and growth of island-like carbon droplets in their case.

The reason for the absence of the peak in the present case on tungsten would be a stronger interaction between the carbon deposit and the substrate than gold. If the deposit has a strong affinity with the substrate, possibly due to the formation of compounds such as WC, a carbon film will rapidly cover the surface at the initial stage of the deposition. The growth after the film formation will be done layer by layer. Therefore, it will not be controlled by the growth of nuclei but by the

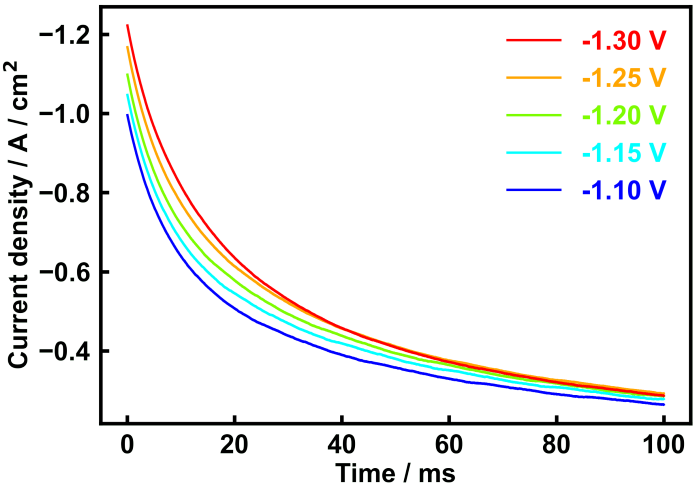

Figure 4.10. Potentiostatic current transient at a tungsten working electrode. (0 - 100 ms) Each potential means an overpotential from the open circuit potential (OCP). Atmosphere: Ar.

diffusion of the reactant.

On a molybdenum and a glassy carbon electrode, similar current-time profiles were obtained and no nucleation phenomenon was observed.

Thus, it was indicated that the nucleation process of carbon on tungsten, molybdenum, and glassy carbon electrodes in the $CaCl_2$-NaCl-$CaCO_3$ system is fairly fast and is solely governed by the diffusion from the initial stage.

It is also worth mentioning that the experimental procedure in this study was not completely ideal. As the state of the electrode surface can be changed after every amperometry, preferably, the electrode must be replaced or, at least, polished every time to get a fresh surface. But in this thesis work, neither of those was possible due to various reasons. One possible solution to this will be discussed in section 6.5.1.

Instead, the working electrode was slightly anodically polarised after each potential step experiment to re-oxidise the deposited carbon. Although this operation may not be as good as getting a completely fresh surface by replacing or polishing, it would be effective to some extent.

4.1.3 Diffusion coefficient of carbonate

Next, the diffusion coefficient of carbonate ion was estimated from current transients at a longer time scale. Figure 4.11 shows the current transient with various applied potentials.

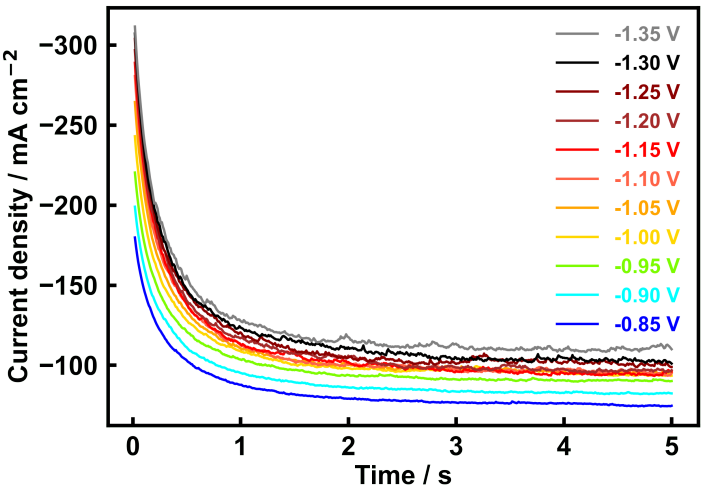

Figure 4.11. Potentiostatic current transient at a tungsten working electrode. (0 - 5 s) Each potential means an overpotential from the open circuit potential (OCP). Atmosphere: Ar.

Around $-1.00 \sim -1.25$ V, potentials that did not affect the current density were observed. This can be considered to be the limiting current density for the carbon deposition reaction in the present system. The current-potential curve at each time is shown in Figure 4.12a. Even though this plot looks like a polarisation curve from an LSV, these points were obtained from the data of the current transient. The existence of the plateau indicates the limiting current for carbon deposition. Thus, in the potential range that gives us the plateau, Cottrell equation is valid and the diffusion coefficient can be calculated. The Cottrell plot is shown in Figure 4.12b.

In order to get rid of the effects of the charging of the double-layer at a very small t and the natural convection at a large t, 1.0 - 3.0 [$s^{-1/2}$] was chosen as the time range. Almost straight lines were obtained. From the regression line of the points at -1.15 V, the slope was calculated as -0.0583 [C $cm^{-2}s^{-1/2}$]. The diffusion coefficient of $CO_3{}^{2-}$ was estimated to be 7.2×10^{-6}[cm^2s^{-1}] from the slope.

It must be noted that the geometry of the working electrode was not a planar disk, but a cylindrical wire in this experiment. Due to the high temperature and the aggressive environment of molten salt, it is not easy to find a suitable material

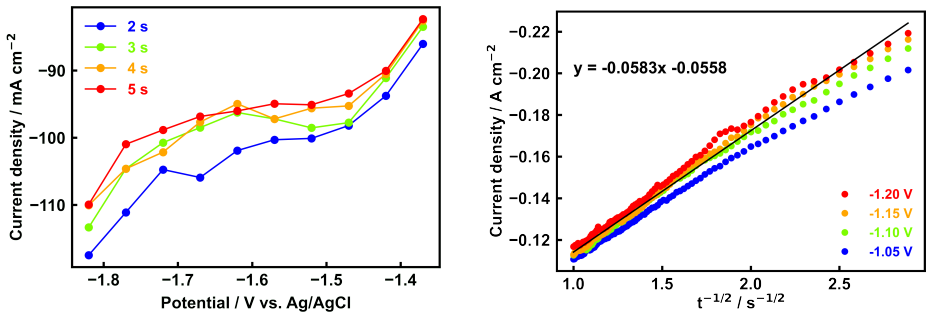

Figure 4.12. (a) i - E plots at each time and (b) Cottrell plot obtained from current transient using a W working electrode.

to cover metal electrodes. Therefore, wire electrodes have also often been used in molten salt electrochemistry owing to their availability.

The theories of diffusion for a cylindrical electrode have been extensively studied.[52], [61] Even though the application of the "normal" Cottrell equation to a cylindrical electrode can give us an error, it can be less than 5% when the following condition is met.[52]

$$\frac{D\tau}{r^2} \leq 3 \times 10^{-3} \tag{48}$$

Here, D is the diffusion coefficient, τ is the time elapsed since the beginning of the electrolysis, and r is the radius of the electrode, which was 1 [mm]. If we assume that D is 1×10^{-5}[cm^2/s] and τ is 1 [s], $D\tau/r^2$ equals 1×10^{-3}. Thus, in the present time range and the geometry of the wire electrode, the criterion to suppress the error within 5% is met.

4.2 Application of an inert anode to the process

4.2.1 Ni-based alloy anode

In the specialisation project (TMT4500) last semester, a nickel-based alloy anode (Ni:Fe:Cu = 45:45:10 wt%) was investigated as a candidate of an inert anode. The results are briefly summarised here for the comparison to the studies done in this thesis. Note that these data are not part of this thesis, but just a citation from a previous work done by the author.

Figure 4.13 shows the current-time curve of potentiostatic electrolysis using a W cathode and a Ni-based alloy anode. The current gradually decreased within 2 hours. Photographs of the alloy anode before and after electrolysis are shown in

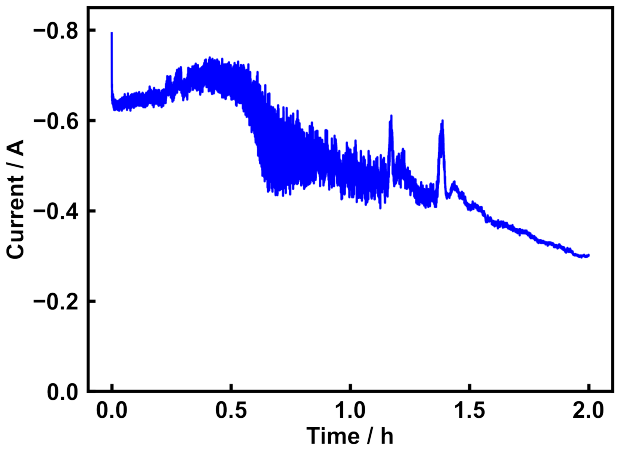

Figure 4.13. Potentiostatic electrolysis using a W cathode and a Nickel-based alloy anode at -1.15 V with respect to OCP. Atmosphere: Ar.[24]

Figure 4.14. The anode was deformed and easily broken after it was retrieved from the melt. Significant corrosion of the anode material was visually confirmed. Also, greenish deposits were observed around the frozen salt bath and on the other electrodes, which indicated the dissolution of the metal species in the alloy. So, the Ni-based alloy anode did not exhibit good stability in molten $CaCl_2$-NaCl-$CaCO_3$. The rapid decrease of the current can be ascribed to the degradation of the anode material.

Figure 4.14. Photographs of nickel-based alloy electrode before (left) and after (right) electrolysis.[24]

4.2.2 Tin oxide anode

In this thesis, an SnO_2 electrode was tested as a candidate of an inert anode. Figure 4.15 shows the current-time curve at a constant potential (-1.15 V with respect to OCP) in molten $CaCl_2$-NaCl-$CaCO_3$.

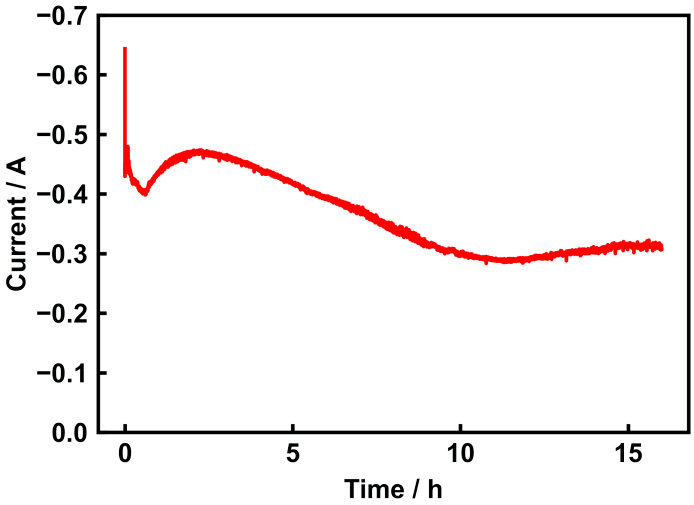

Figure 4.15. Potentiostatic electrolysis using W cathode and SnO_2 anode at -1.15 V with respect to OCP. Atmosphere: Ar.

After the current spike due to the charging of the electric double layer, the current gradually increased until around 2 hours. This is attributed to the increase of the active surface area due to the deposition of carbon on the cathode. After this, the current started to decrease. The probable explanation would be the decrease of carbonate concentration in the melt. The current became steady after 10 hours. Since the crucible material was graphite, and it can be burned by oxygen gas produced at the anode, some CO_2 could be captured in the melt and carbonate could be continuously resupplied to the melt. This can be the reason why the current ended up with a steady profile rather than continuously decreasing.

The appearance of the SnO_2-based anode before and after electrolysis is shown in Figure 4.16. No significant damage was visually confirmed apart from a slight change of the colour in the immersed area. So, judging from the stable current-time profile and the state of the electrode, it was shown that SnO_2-based anode showed better stability than the Ni-based alloy anode in molten $CaCl_2$-NaCl-$CaCO_3$. Since this result was promising, SnO_2 electrodes were used for the further experiments.

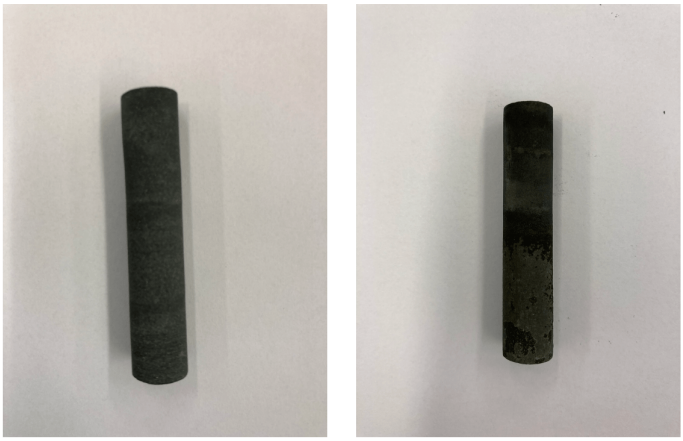

Figure 4.16. Photographs of the SnO_2-based anode before (left) and after (right) electrolysis.

4.3 CO_2 capture using simulated exhaust from industrial processes

4.3.1 Voltammetry under CO_2 gas flow

First, voltammetry under pure CO_2 atmosphere was performed. The cyclic voltammograms using a tungsten working electrode in $CaCl_2$-NaCl-CaO under pure CO_2 flow are shown in Figure 4.17. Here, no carbonate was added. Instead, 1 mol% of CaO was present to capture CO_2 gas as ${CO_3}^{2-}$.

When CO_2 gas was injected into the system, the shape of the voltammogram drastically changed. It showed a larger current and a line-crossing was observed, which indicates the increase in the surface area of the electrode. Since this behaviour was not observed under Ar gas flow, this can be ascribed to the deposition of carbon.

Next, aiming at the application to the industrial processes, a diluted CO_2 gas was employed to supply carbon to the system. Here, 1 vol% of CO_2 gas was used, which is a typical CO_2 concentration of the flue gas from aluminium electrolysis. Figure 4.18 shows cyclic voltammograms under pure CO_2 gas flow or diluted CO_2 gas flow.

When the concentration of CO_2 was decreased, the cathodic peak around -1.3 V (vs. AgCl) became smaller and clearer. This could be due to the limited supply of ${CO_3}^{2-}$. The peak position is almost identical to the peak C2 in Figure 4.3b. Although it was small, a cathodic peak corresponding to the peak C1 was also observed. Thus, it was confirmed that reduction of carbonate was taking place even under a low concentration of CO_2.

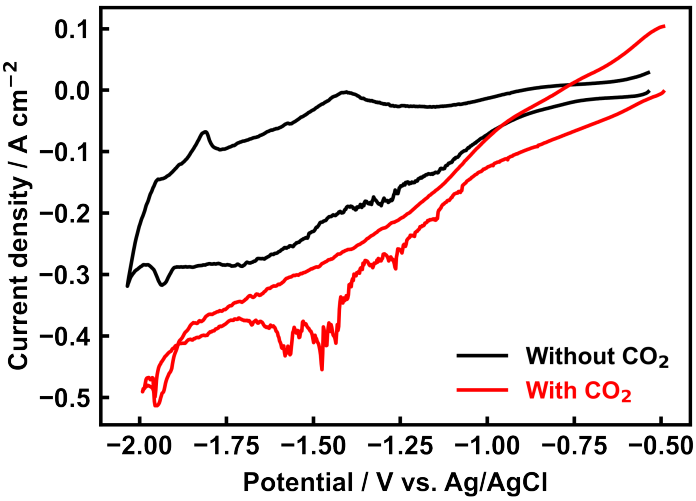

Figure 4.17. Cyclic volatmmograms on a W working electrode with (red) and without (black) CO_2 bubbling in molten $CaCl_2$-NaCl-CaO (80 mol%:20 mol% + 1 mol%). Scan rate: 500 mV/s, flow gas: pure CO_2 (100 mL/min).

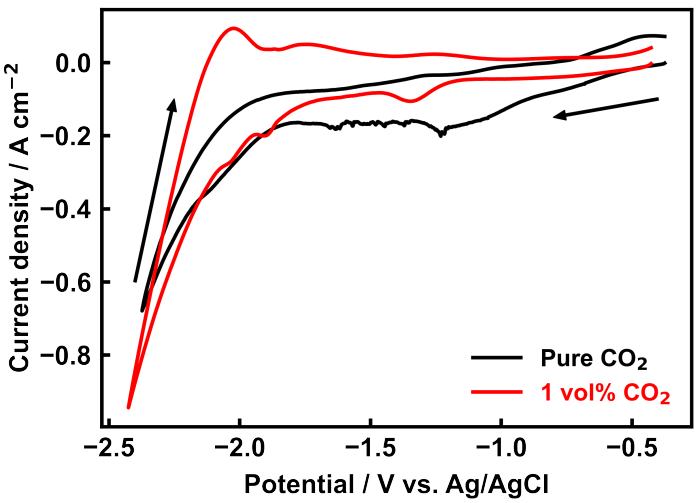

Figure 4.18. Cyclic voltammograms using a W working electrode in molten $CaCl_2$-NaCl-CaO (80 mol%:20 mol% + 1 mol%) under pure CO_2 gas and 1 vol% CO_2 gas.

Also, the effect of CaO added to the system was further investigated. According to the theory, oxide ions resulting from CaO are playing a role to capture CO_2 gas. To confirm this effect, a blank experiment without calcium oxide was also carried out. Figure 4.19 shows cyclic voltammograms in $CaCl_2$-NaCl (80 mol%:20 mol%) molten salt with and without CO_2 gas. Surprisingly, despite the absence of oxide in the system, a similar current-potential profile to the voltammogram under pure CO_2 was observed.

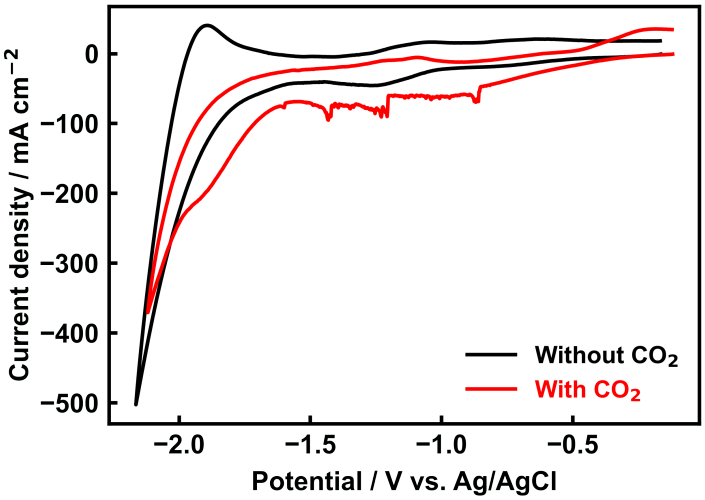

Figure 4.19. Cyclic volatmmograms on a Mo working electrode with (red) and without (black) CO_2 bubbling in molten $CaCl_2$-NaCl (80 mol%:20 mol%). Scan rate: 500 mV/s, flow gas: pure CO_2 (100 mL/min).

There are two possibilities why carbon deposition happened even without CaO in the melt. One reason may be the direct reduction of CO_2 gas.

$$CO_2 + 4e^- = C + 2O^{2-} \tag{49}$$

Novoselova *et al.* confirmed carbon deposition in NaCl-KCl molten salt under 1.0 MPa CO_2 atmosphere.[62] Since no oxide was added to the system, the authors assumed that the carbon dioxide was directly converted into carbon according to Eq. 49.

The other possibility is the existence of a small amount of impurities in $CaCl_2$-NaCl salt. Since $CaCl_2$ has a hygroscopic nature, it can easily absorb moisture in the atmosphere. Even though considerable attention was paid to removing the moisture from the salts in the series of experiments, a small amount of water could

still remain in the system, which forms oxide and ends up as carbonate by reacting with CO_2 gas. Furthermore, if a single carbonate ion is reduced into carbon, it releases three oxide ions according to the following equation.

$$CO_3{}^{2-} + 4e^- = C + 3O^{2-}$$

Due to the very small amount of oxide ions in the system, it is not likely for the oxide ions to be oxidised at the anode. Therefore, at a low oxide concentration, chlorine evolution would be the dominant anodic reaction.

$$2Cl^- = Cl_2 + 2e^-$$

The newly formed oxide ions start to absorb CO_2 and each of them forms carbonate.

$$CO_2 + O^{2-} = CO_3{}^{2-}$$

Then, the carbonate ions will be reduced and oxide ions will be newly formed again. Repeating these processes, the amount of oxide (carbonate) will be built up even if the initial concentration of oxide is very small. This series of processes could persist until it is offset by the consumption of oxide ions due to oxygen evolution reaction.

The real picture of the carbon deposition process without oxide may even be the sum of the two possibilities above. In other words, oxide ions are formed by direct reduction and/or small amount of carbonate resulting from the impurities, and then, the concentration of oxides can be built up until it reaches a certain point. Further investigation regarding the oxide concentration and its effect will be desired.

4.3.2 Electrolysis under CO_2 gas flow

Since the voltammetry indicated that carbon deposition was taking place with CO_2 gas supply, prolonged electrolyses were performed to get an observable amount of carbon product. Figure 4.20 is showing a current-time curve of potentiostatic electrolysis under pure CO_2 gas flow.

The current was increased until around 10 hours. The main reason for this will be the increase of the active surface area owing to the carbon deposition on the cathode. After 10 hours, the current was almost steady around -1.7 A and did not increase anymore. Two reasons can be considered for this. The first possibility is the limit of the mass transport. CO_2 gas was supplied at 100 mL/min of flow rate, which corresponds to 68 μmol/s. However, all the CO_2 bubbled in the melt is not necessarily absorbed by CaO due to the equilibrium of $CaCO_3 = CaO + CO_2(g)$. So, there should be a limit of how much CO_2 can be captured and utilised for the

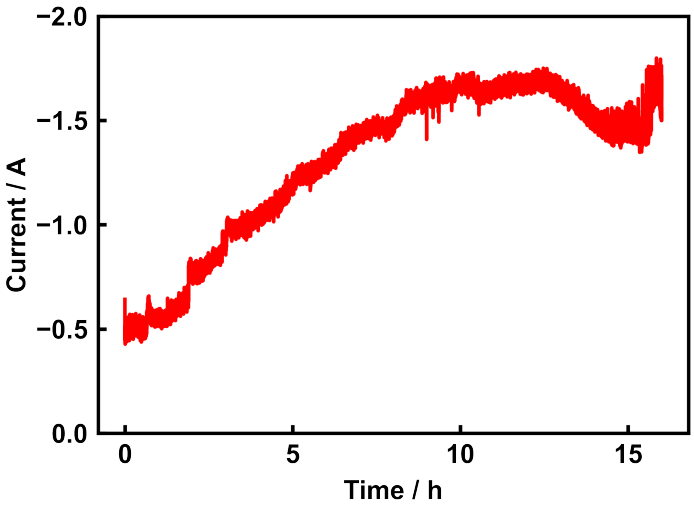

Figure 4.20. Potentiostatic electrolysis using a W cathode and an SnO_2 anode at -1.15 V with respect to OCP. Cathode: W, Anode: SnO_2, Flow gas: pure CO_2, Flow rate: 100 mL/min.

reaction. In addition to the diffusion of carbonate, the molten salt was stirred by bubbling in this case. Still, it does not necessarily mean that all the dissolved CO_2 can be supplied to the cathode surface.

The second possibility is that the increase of surface area can be offset by the decrease of the surface area resulting from detaching of the product. This can be caused perhaps by CO formation, which is one of the side reactions in this system. Further investigation including gas analysis and visual observation of the process would be needed.

Figure 4.21 shows the photographs of the cathode and the anode after the prolonged electrolysis under pure CO_2 atmosphere. On the tungsten cathode, carbon deposition was visually confirmed. The carbon product was washed and collected. The yield of the carbon product was 1.5%. The reasons for the low yield would be due to the CO formation and the detaching of carbon products during the reaction. In fact, some carbon powder was also confirmed at the bottom of the crucible. The design of the electrode and the collection process shall be optimised in further work. It will be discussed in Chapter 6.

On the other hand, no significant corrosion or mechanical damage was not visually confirmed on the SnO_2-based anode. The only difference was the change of the colour in the dipped area in the melt, as with the case of the electrolysis in molten $CaCl_2$-NaCl-$CaCO_3$. Thus, the SnO_2-based anode showed a fairly good stability

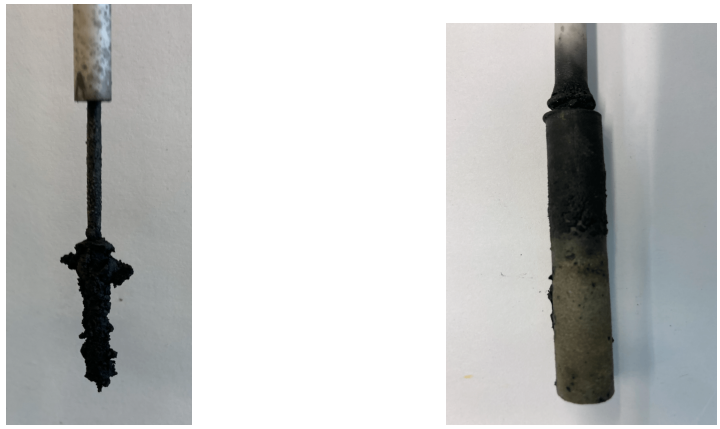

(a) **(b)**

Figure 4.21. Photographs of the electrodes after the prolonged electrolysis under pure CO_2 gas flow: (a)W cathode and (b)SnO_2 anode.

in electrolysis under the CO_2 gas flow condition as well.

SEM images of the carbon product are shown in Figure 4.22. The majority of the sample was small shapeless particles. But some part of the product had nano-tubuler structures. The mechanism of the formation of such structure will be surveyed and it will be important to control the selectivity of the final product.

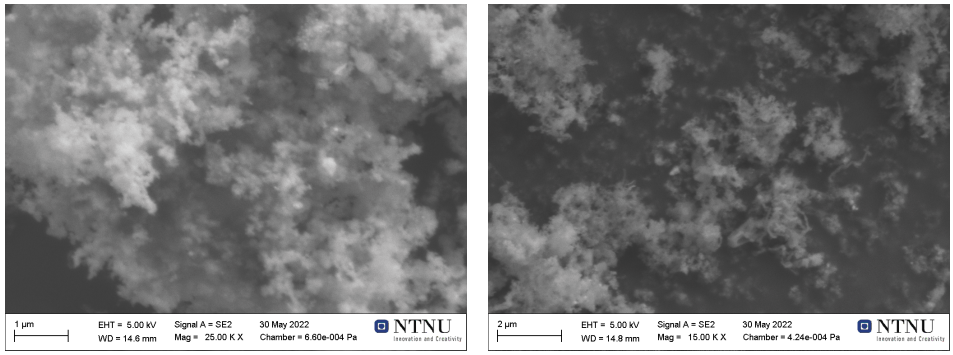

(a) **(b)**

Figure 4.22. SEM images of the carbon product obtained from potentiostatic electrolysis under pure CO_2 gas flow. (a) Typical image of the sample and (b) Part including tubular nanostructures.

For comparison, potentiostatic electrolysis under pure CO_2 using a W cathode and a graphite anode was also conducted. The current profile was similarly stable and

a product with some nanostructures was obtained. Graphitic structures were also observed in the product, but the possibility that it came from the anode material could not be ruled out. The data will be found in Appendix A.

Finally, potentiostatic electrolysis employing 1 vol% CO_2 was conducted.(Figure 4.23) The current was steady and it slightly increased over time, which can be due to the increase of the surface area. Although the profile looks noisier than Figure 4.20, this is merely because of the smaller current and the magnification.

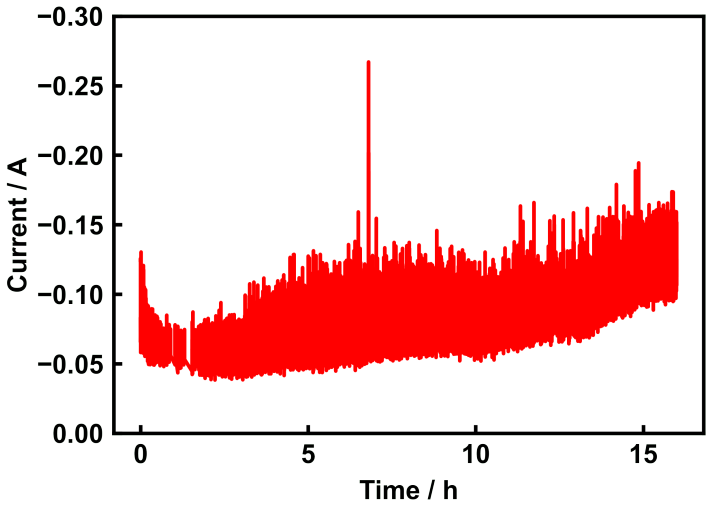

Figure 4.23. Potentiostatic electrolysis using W cathode and SnO_2 anode at -1.15 V with respect to OCP. Cathode: W, Anode: SnO_2, Flow gas: 1 vol% CO_2, Flow rate: 300 mL/min.

Here, the flow rate was changed from 100 mL/min to 300 mL/min. This is due to the limitation of the mass flow controller used in the experiment. Since the minimum volume that the controller can handle was 3 mL, there was no choice but to increase the total flow rate to make the concentration 1 vol%.

The photographs of the electrodes are shown in Figure 4.24. Even though some carbon deposit on the cathode surface was visually confirmed, the amount was small and collection of the product was unsuccessful. Some carbon powder was confirmed in the bottom of the crucible, indicating the loss from the cathode surface during the process.

The tin oxide-based anode showed a good durability in this case as well. Although slight change of the colour was observed, there was no cracking or any other mechanical damage. Further studies are desired to determine the corrosion rate and

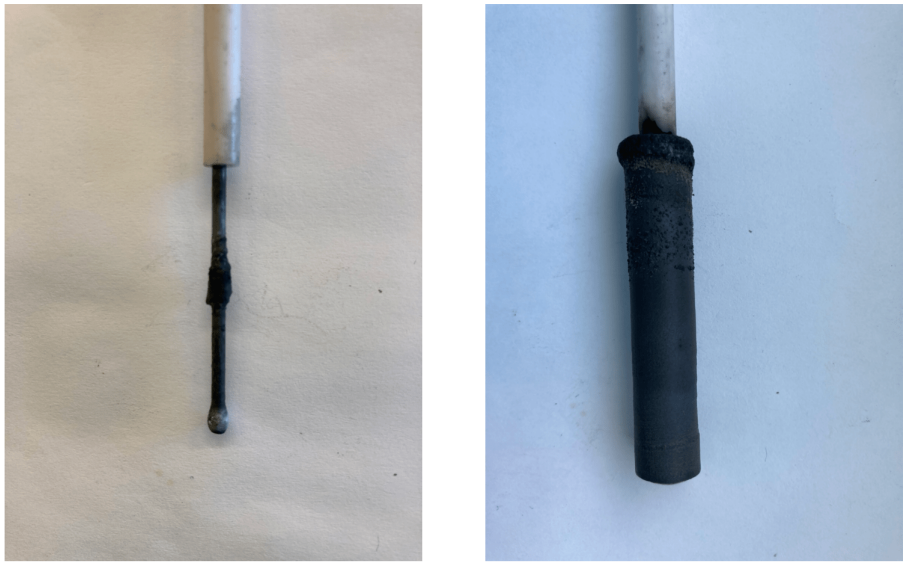

Figure 4.24. Photographs of the electrodes after prolonged electrolysis under 1 vol% CO_2 flow. Left: W cathode and right: SnO_2 anode.

the chemical state of the surface.

5 Conclusions

The cathodic behaviour of CO_3^{2-} in molten $CaCl_2$-NaCl-$CaCO_3$ on various electrode materials was investigated. Voltammetry showed one cathodic peak on a glassy carbon and a graphite working electrode apart from the deposition peak of Ca and/or Na metal. The current-potential curves exhibited a characteristic loop-shaped hysteresis and it indicated the increase of the active surface area of the electrode, which can be ascribed to the carbon deposition.

On tungsten and molybdenum electrodes, two distinctive cathodic peaks were observed in addition to the reduction peak of alkali/alkaline earth metals. It was suggested that the reduction of carbonate was taking place via the following steps: i) formation of CO_2^{2-} and ii) deposition of carbon. Potentiostatic electrolyses were performed at the two cathodic peaks. As a result, carbon deposition was obtained at the second cathodic peak, while no solid product was observed at the first one. This result endorses the suggested two-step reaction mechanism.

The nucleation process of carbon was studied by current transient methods. No characteristic peak current originating from the growth of nuclei was observed. The result indicated the fast deposition process of carbon on tungsten and it can be attributed to the strong affinity between carbon and tungsten.

The diffusion coefficient of CO_3^{2-} was estimated to be $7.2 \times 10^{-6}[\mathrm{cm^2 s^{-1}}]$ at 800°C by chronoamperometry.

Application of inert anodes to the process was also attempted. An SnO_2-based anode showed a better performance than a Ni-based alloy anode. It showed a steady current for 16 hours under potentiostatic electrolysis in molten $CaCl_2$-NaCl-$CaCO_3$. Apart from a slight change of the colour, significant damage to the electrode such as exfoliation or crack was not observed.

Voltammetric studies were performed under CO_2 gas flow, aiming at the application to the industrial processes. Pure CO_2 and diluted CO_2 gas (1 vol%) were injected as the carbon source. In either case, a new cathodic peak was confirmed. Judging from the similar peak position to the case of CO_3^{2-} reduction, it was identified as carbon deposition.

Long-term electrolyses under simulated exhausts were carried out. Deposition of carbon was confirmed under CO_2 gas flow. SEM images showed that some of the collected products had nanotube-like structures.

6 Further work

6.1 Experimental conditions affecting the final product

As it was introduced in Chapter 2, the carbon product from the CO_2 electrolysis process varies depending on the reaction conditions. Due to the limitation of time, not so many reaction conditions were attempted. Here, some of the possibilities of factors that can be changed in further work are presented.

6.1.1 Operating temperature and salt composition

First of all, the operating temperature of the process is one of the most important factors. From the thermodynamic calculation in Chapter 2 and Appendix C., the standard potentials of carbon deposition and CO formation are very close around 800°C. As a trend, the higher the temperature is, the more easily CO can be produced. Thus, lowering the operating temperature can be beneficial to minimise the CO formation and maximise the yield of solid carbon.

Also, higher temperatures can be detrimental to the carbon capture reaction either.

$$CO_2 + O^{2-} = {CO_3}^{2-}$$

The Gibbs energy change of this reaction becomes more positive when the temperature is increased. (See Table:D.1). That is, carbonate becomes likely to decompose into CO_2 and O^{2-}.

In order to lower the operating temperature, the salt composition may be reconsidered. Figure 6.1 shows the phase diagram of $CaCl_2$-NaCl system.[63] The liquidus temperature of this systems can reach the minimum when the molar ratio is around 0.52:0.48. Increasing the amount of NaCl can be helpful when lower temperatures are attempted.

6.1.2 Cathode materials

The choice of the cathode hugely affects the results. Although there are numerous reports regarding the effect of the cathode material choice, any unified overview has never been obtained.

In this study, W, Mo, glassy carbon, and graphite electrodes were chosen as the working electrode (cathode in the case of electrolysis). As for electrolytic studies, tungsten was mainly employed and not so many insights into the cases for other cathodes were obtained. This could be one of the next steps. Among them, use of graphite cathodes is of particular interest, as it is well known that graphite cathodes often create carbon nanofibres/nanotubes, owing to the intercalation of alkali

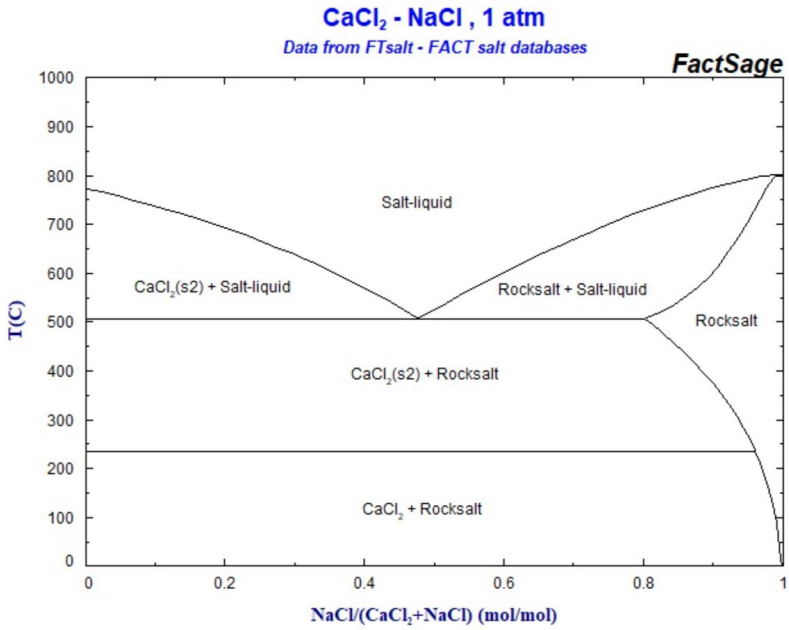

Figure 6.1. Phase diagram of $CaCl_2$-NaCl salt.[63]

metals into graphitic sheets.

For the observation of nucleation processes, the use of gold electrodes can be an option. As discussed in section 4.1.2, any nucleation process was not observed on W, Mo, or glassy carbon electrodes. These results were quite different from the work done by Massot *et al.*[59], and it was attributed to the choice of the cathode material. Although the electrolyte was different from their case, if we employ Au as the cathode material, it might be possible to get new insights into the nucleation process of carbon in molten $CaCl_2$-NaCl-$CaCO_3$.

6.1.3 Anode materials

Anode materials are as important as cathode materials. Even though it was demonstrated that an SnO_2-based anode was fairly inert and was sufficiently durable even for prolonged electrolysis, the further investigation is still needed. The state of the electrode surface shall be further studied by using microscopic techniques. Also, the chemical state of the electrode could have been changed. Analysis using XRD and XPS may be the options.

Other anode materials need to be continuously sought out. This is a never-ending challenge in molten salt electrochemistry. As it was introduced in Chapter 2,

alternatives to SnO_2-based anodes have been developed recently. Although Ru-containing anodes show good performances, Ru is a rare element and too expensive. So, novel anode materials with low cost and fairly high performance must be developed. The number of reports regarding new inert anode materials such as composite oxide anodes is still limited, and there is a lot of room to be pioneered.

Instead of inert anodes, consumable anodes such as Ni can give us different possibilities. It is known that it could be slowly dissolved in molten carbonate and deposited on the cathode during the process.[35] Then, the deposited nanoparticles work as nucleation sites for the growth of carbon nanomaterials such as carbon nanotubes. However, the environment of chloride molten salts is generally more aggressive than carbonate. The material choice and the controlling of moderate dissolution of metal may be more challenging.

6.2 Further investigation of the products

Further characterisation of the products is of great importance. In this thesis, sufficient attention was not paid to the properties of the carbon products, as the main focus was on the electrochemical aspects of the process. However, for a better understanding of the process and creation of new synthesis routes for carbon materials, more information regarding the products is needed.

In addition to SEM images, observation using TEM may be helpful in some cases. Since it enables us to obtain the information inside the samples, it will make it possible to observe the graphitic layers in the carbon products and to give us valuable information, such as the interplanar distance of (002) planes.

Further structural analysis using X-ray diffraction and Raman spectroscopy will be needed. Although some tubular-shaped structure was obtained in this work, it is necessary to validate the structure by combining several different methods. Since there have been numerous previous structural studies on carbon materials, it is possible to compare the result with them. Such insights will also be beneficial to validate the results and determine the next direction of the study.

Analysis of gaseous products is also desired. As it was discussed, CO is the main by-product at the cathode. On the other hand, oxygen is supposed to be produced at the anode. But with the current experimental set-up, it is not possible to get any information regarding gasses that are actually produced from the system. In order to get insights into the current efficiency and the side reactions happening there, gas analysis using a gas chromatograph will be needed. The information from it will allow us to tune the reaction condition and optimise it to be able to maximise the current efficiency for solid carbon products. Particularly, the relation between the current densities and products is of interest.

6.3 Visual observation of carbon deposition process

The series of experiments were done in an electric furnace that was completely covered with a wall and insulating materials. Thus, it has been impossible to see the inside of the furnace and observe how the carbon deposition was taking place. This problem can be circumvented by the use of a so-called "see-through" furnace, where a quartz window is equipped and it allows us to look inside the furnace under operation. Observation of gas evolution and movement of deposited carbon would give us new insights into the process.

6.4 Cell design

The configuration of electrodes is one of the most important matters to be considered. In this study, all the electrodes were vertically aligned, apart from the graphite crucible (anode). As it was revealed, the deposited carbon can easily be detached. Then, the powder floats or sinks, depending on the density of the product. If the cathode is aligned horizontally, it can be helpful to assist the carbon products to stick to the electrode.

The anode-cathode distance is an important factor in metal production. In the research field of CO_2 electrolysis in molten salt, however, it has not been discussed well so far. Generally, the interpolar distance can largely affect the current efficiency of the products. So, it might be interesting to see its effects on CO_2electrolysis in further work.

It is widely believed that the CO_2 electrolysis using molten salt can easily be scalable by simply enlarging the size of the components of the cell.[19] But this has not been tested at all and confirmed. After thorough optimisation of the experimental conditions and cell designs, this also must be examined.

6.5 Improvement of experimental procedures

In order to improve the quality of data, reproducibility, and convenience, some ideas can be suggested.

The items written in this section are not necessarilyy about general insights into the academic aspects of the research, but about very specific and local situations in our research environment that we might be able to improve in the near future.

6.5.1 Conducting all the procedures in a glove box

Part of this thesis was focusing on the carbon deposition process on electrodes such as tungsten. Since the electrode gets deposition on its surface and the state can be

changed after every sweep, it is ideal to restore the state of it every time. In this thesis work, an anodic polarisation was typically performed after cathodic sweeps. The purpose was to dissolve the carbon deposition and obtain a fresh surface again. However, there was no guarantee that the deposition was completely removed or not, as the inside is invisible during the experiment. So, ideally, the electrode should be replaced every time with a new one or, at least, should be polished.

It can be difficult to change the electrode every time, in terms of the cost and the availability. Polishing could be a better choice, but since the electrode can be immediately oxidised by air when it was taken out of the furnace, it is also not easy. However, if we could conduct all the experiments in a glove box filled with an inert gas, the electrodes will not be burned and polishing will become a realistic operation.

This will also be helpful to maintain the purity of the salts. Although the salts were dried before use to remove the moisture, the weighing process was done under ambient temperature in air. So, there is still room for moisture to be absorbed again. If every process after drying can be done in glove box, we will be able to minimise such possibilities.

6.5.2 Choice of crucible material

In this thesis work, graphite crucibles were used for the entire experiments mainly due to the availability. But since it can be burned by the evolved oxygen and can provide CO_2 to the system, the crucible itself could become a carbon source. Since the aim of this process is to utilise CO_2 gas as the carbon source, this is not a good situation. Furthermore, the product of the electrolysis is also carbon. In order to ensure that the product comes from CO_2, any carbon materials should ideally be eliminated from the system. Therefore, it is recommended to use crucibles made with another material such as alumina in future work.

6.5.3 Mass flow controller

Due to the limitation of the capability of the mass flow controller, it was not easy to achieve a low CO_2 concentration in the flue gas. The only option was to increase the total flow rate of the gas mixture, but a high flow rate is not necessarily a good option. There are two reasons. First, if the flow rate was too fast, it can create disturbance in the melt and it promotes the carbon deposit coming off, which can result in the loss of the product. Second, it splashes the melt with carbon products and makes the furnace dirty. To avoid these, in future work, a mass flow controller to deal with a smaller flow rate will be desired.

7 Acknowledgement

As with the last semester, my project work was supported by so many people.

First, I would like to show my gratitude to Dr. Karen Sende Osen of SINTEF. She gave me enormous help throughout the year with the actual laboratory activities as the room responsible. Her plentiful experiences and deep knowledge in molten salt electrochemistry have been inevitable for my work. She also often kindly cared about me and cheered me up when we met in the lab. I also thank Dr. Bo Qin and Mr. Kamaljeet Singh for the fruitful discussions and other activities. Since they have been the only people who are working under the same supervisor, there were many chances for us to meet and do something together.

All the support from the technical staff in K2 is also greatly appreciated. I would like to thank Dr. Anita Storsve for her kind support with getting necessities for my laboratory work. Dr. Marthe Folstad always readily offered me items that I needed. Dr. Pei Na Kui helped me a lot with establishing a new CO_2 gas flow system.

I am grateful to other staff in the department and the faculty as well. Dr. Yingda Yu kindly helped me with operating SEM-EDS. Mr. Aksel Alstad greatly contributed to fabricating my electrodes.

I would like to appreciate the help from Professor Svein Sunde and Dr. Wojciech Gebarowski with the noise problem during my electrochemical measurements. They could spend their precious time on investigating the problem for me. Professor Frode Seland also gave me some advice on this matter, which is also appreciated.

I would also like to thank Dr. Henrik Gudbrandsen and Dr. Babak Khalaghi of SINTEF for helping me with establishing and operating the gas flow system.

8 References

[1] R. Lindsey and L. Dahlman. "Climate change: Global temperature." (2021), [Online]. Available: https://www.climate.gov/news-features/understanding-climate/climate-change-global-temperature (visited on 03/31/2022).

[2] M. Oppenheimer, B. Glavovic, J. Hinkel, *et al.*, "Sea level rise and implications for low lying islands, coasts and communities," 2019.

[3] IPCC and C. W. Team, *Contribution of working groups i, ii and iii to the fifth assessment report of the intergovernmental panel on climate change*, 2014.

[4] H. Ritchie and M. Roser. "CO_2 Emissions." (2020), [Online]. Available: https://ourworldindata.org/co2-emissions (visited on 05/05/2022).

[5] P. Tans and R. Keeling. "Trends in atmospheric carbon dioxide." (2021), [Online]. Available: https://gml.noaa.gov/ccgg/trends/monthly.html (visited on 05/05/2021).

[6] D. Lüthi, M. Le Floch, B. Bereiter, *et al.*, "High-resolution carbon dioxide concentration record 650,000–800,000 years before present," *nature*, vol. 453, no. 7193, pp. 379–382, 2008.

[7] D. Lüthi, M. Le Floch, B. Bereiter, *et al.* "Epica dome c - 800kyr CO_2 data." (2008), [Online]. Available: https://www.ncei.noaa.gov/access/paleo-search/study/6091 (visited on 05/05/2022).

[8] J. Gibbins and H. Chalmers, "Carbon capture and storage," *Energy policy*, vol. 36, no. 12, pp. 4317–4322, 2008. DOI: https://doi.org/10.1016/j.enpol.2008.09.058.

[9] R. S. Haszeldine, "Carbon capture and storage: How green can black be?" *Science*, vol. 325, no. 5948, pp. 1647–1652, 2009. DOI: https://doi.org/10.1126/science.1172246.

[10] M. E. Boot-Handford, J. C. Abanades, E. J. Anthony, *et al.*, "Carbon capture and storage update," *Energy & Environmental Science*, vol. 7, no. 1, pp. 130–189, 2014. DOI: https://doi.org/10.1039/C3EE42350F.

[11] D. T. Whipple and P. J. Kenis, "Prospects of CO_2 utilization via direct heterogeneous electrochemical reduction," *The Journal of Physical Chemistry Letters*, vol. 1, no. 24, pp. 3451–3458, 2010. DOI: https://doi.org/10.1021/jz1012627.

[12] S. Ma, P. J. Kenis, *et al.*, "Electrochemical conversion of CO_2 to useful chemicals: Current status, remaining challenges, and future opportunities," *Current Opinion in Chemical Engineering*, vol. 2, no. 2, pp. 191–199, 2013. DOI: https://doi.org/10.1016/j.coche.2013.03.005.

[13] J. L. White, M. F. Baruch, J. E. Pander III, *et al.*, "Light-driven heterogeneous reduction of carbon dioxide: Photocatalysts and photoelectrodes," *Chemical reviews*, vol. 115, no. 23, pp. 12 888–12 935, 2015. DOI: https://doi.org/10.1021/acs.chemrev.5b00370.

[14] G. H. Aylward and T. J. V. Findlay, *SI chemical data, 7th edition*. New York, Wiley, 2013.

[15] R. O. Suzuki, K. Ono, and K. Teranuma, "Calciothermic reduction of titanium oxide and in-situ electrolysis in molten $CaCl_2$," *Metallurgical and Materials Transactions B*, vol. 34, no. 3, pp. 287–295, 2003. DOI: https://doi.org/10.1007/s11663-003-0074-1.

[16] H. V. Ijije, R. C. Lawrence, and G. Z. Chen, "Carbon electrodeposition in molten salts: Electrode reactions and applications," *RSC advances*, vol. 4, no. 67, pp. 35 808–35 817, 2014.

[17] M. A. Hughes, J. A. Allen, and S. W. Donne, "Carbonate reduction and the properties and applications of carbon formed through electrochemical deposition in molten carbonates: A review," *Electrochimica Acta*, vol. 176, pp. 1511–1521, 2015. DOI: https://doi.org/10.1016/j.electacta.2015.07.134.

[18] D. Chery, V. Lair, and M. Cassir, "Overview on CO_2 valorization: Challenge of molten carbonates," *Frontiers in Energy Research*, vol. 3, p. 43, 2015. DOI: https://doi.org/10.3389/fenrg.2015.00043.

[19] W. Weng, L. Tang, and W. Xiao, "Capture and electro-splitting of CO_2 in molten salts," *Journal of Energy Chemistry*, vol. 28, pp. 128–143, 2019.

[20] Y. Chen, M. Wang, J. Zhang, J. Tu, J. Ge, and S. Jiao, "Green and sustainable molten salt electrochemistry for the conversion of secondary carbon pollutants to advanced carbon materials," *Journal of Materials Chemistry A*, vol. 9, no. 25, pp. 14 119–14 146, 2021. DOI: https://doi.org/10.1039/D1TA03263A.

[21] E. Freidina and D. Fray, "Study of the ternary system $CaCl_2 - NaCl - CaO$ by dsc," *Thermochimica acta*, vol. 354, no. 1-2, pp. 59–62, 2000.

[22] Z. Chen, J. Liu, Z. Yu, and K.-C. Chou, "Electrical conductivity of $CaCl_2 - KCl - NaCl$ system at 1080 k," *Thermochimica acta*, vol. 543, pp. 107–112, 2012. DOI: https://doi.org/10.1016/j.tca.2012.05.007.

[23] R. Barnett, K. T. Kilby, and D. J. Fray, "Reduction of tantalum pentoxide using graphite and tin-oxide-based anodes via the FFC-cambridge process," *Metallurgical and materials transactions B*, vol. 40, no. 2, pp. 150–157, 2009. DOI: https://doi.org/10.1007/s11663-008-9219-6.

[24] Y. Takahashi, "Specialisation project report: Carbon capture and recovery by molten salts electrochemistry," *NTNU*, 2021.

[25] Y. Ito, T. Shimada, and H. Kawamura, "Electrochemical formation of thin carbon film from molten chloride system," *ECS Proceedings Volumes*, vol. 1992, no. 1, p. 574, 1992. DOI: https://doi.org/10.1149/199216.0574PV.

[26] M. Deanhardt, K. H. Stern, and A. Kende, "Thermal decomposition and reduction of carbonate ion in fluoride melts," *Journal of the Electrochemical Society*, vol. 133, no. 6, p. 1148, 1986. DOI: https://doi.org/10.1149/1.2108802.

[27] V. Kaplan, E. Wachtel, K. Gartsman, Y. Feldman, and I. Lubomirsky, "Conversion of co2 to co by electrolysis of molten lithium carbonate," *Journal of the Electrochemical Society*, vol. 157, no. 4, B552, 2010.

[28] F. Matsuura, T. Wakamatsu, S. Natsui, T. Kikuchi, and R. O. Suzuki, "Co gas production by molten salt electrolysis from CO_2 gas," *ISIJ International*, vol. 55, no. 2, pp. 404–408, 2015. DOI: 10.2355/isijinternational.55.404.

[29] M. Ingram, B. Baron, and G. Janz, "The electrolytic deposition of carbon from fused carbonates," *Electrochimica Acta*, vol. 11, no. 11, pp. 1629–1639, 1966. DOI: https://doi.org/10.1016/0013-4686(66)80076-2.

[30] G. Janz and A. Conte, "Potentiostatic polarization studies in fused carbonates—i. the noble metals, silver and nickel," *Electrochimica Acta*, vol. 9, no. 10, pp. 1269–1278, 1964. DOI: https://doi.org/10.1016/0013-4686(64)87003-1.

[31] D. Fray, "Molten salts and energy related materials," *Faraday Discussions*, vol. 190, pp. 11–34, 2016. DOI: https://doi.org/10.1039/C6FD00090H.

[32] H. Kawamura and Y. Ito, "Electrodeposition of cohesive carbon films on aluminum in a $LiCl - KCl - K_2CO_3$ melt," *Journal of applied electrochemistry*, vol. 30, no. 5, pp. 571–574, 2000. DOI: https://doi.org/10.1023/A:1003927100308.

[33] L. Massot, P. Chamelot, F. Bouyer, and P. Taxil, "Electrodeposition of carbon films from molten alkaline fluoride media," *Electrochimica Acta*, vol. 47, no. 12, pp. 1949–1957, 2002. DOI: https://doi.org/10.1016/S0013-4686(02)00047-6.

[34] W. K. Hsu, J. Hare, M. Terrones, H. Kroto, and D. Walton, "Condensed-phase nanotubes," *Nature*, vol. 377, p. 687, 1995.

[35] J. Ren, F.-F. Li, J. Lau, L. González-Urbina, and S. Licht, "One-pot synthesis of carbon nanofibers from co2," *Nano letters*, vol. 15, no. 9, pp. 6142–6148, 2015.

[36] J. Ren and S. Licht, "Tracking airborne CO_2 mitigation and low cost transformation into valuable carbon nanotubes," *Scientific Reports*, vol. 6, no. 1, pp. 1–11, 2016. DOI: https://doi.org/10.1038/srep27760.

[37] W. Weng, B. Jiang, Z. Wang, and W. Xiao, "In situ electrochemical conversion of co2 in molten salts to advanced energy materials with reduced carbon emissions," *Science advances*, vol. 6, no. 9, eaay9278, 2020. DOI: https://doi.org/10.1126/sciadv.aay9278.

[38] L. Hu, Y. Song, S. Jiao, *et al.*, "Direct conversion of greenhouse gas CO_2 into graphene via molten salts electrolysis," *ChemSusChem*, vol. 9, no. 6, pp. 588–594, 2016. DOI: https://doi.org/10.1002/cssc.201501591.

[39] A. R. Kamali and D. J. Fray, "Preparation of nanodiamonds from carbon nanoparticles at atmospheric pressure," *Chemical Communications*, vol. 51, no. 26, pp. 5594–5597, 2015. DOI: https://doi.org/10.1039/C5CC00233H.

[40] A. R. Kamali, "Nanocatalytic conversion of CO_2 into nanodiamonds," *Carbon*, vol. 123, pp. 205–215, 2017. DOI: https://doi.org/10.1016/j.carbon.2017.07.040.

[41] B. Deng, X. Mao, W. Xiao, and D. Wang, "Microbubble effect-assisted electrolytic synthesis of hollow carbon spheres from CO_2," *Journal of Materials Chemistry A*, vol. 5, no. 25, pp. 12 822–12 827, 2017. DOI: https://doi.org/10.1039/C7TA03606J.

[42] X. Liu, J. Ren, G. Licht, X. Wang, and S. Licht, "Carbon nano-onions made directly from CO_2 by molten electrolysis for greenhouse gas mitigation," *Advanced Sustainable Systems*, vol. 3, no. 10, p. 1 900 056, 2019. DOI: https://doi.org/10.1002/adsu.201900056.

[43] X. Wang, G. Licht, X. Liu, and S. Licht, "One pot facile transformation of CO_2 to an unusual 3-d nano-scaffold morphology of carbon," *Scientific Reports*, vol. 10, no. 1, pp. 1–12, 2020. DOI: https://doi.org/10.1038/s41598-020-78258-6.

[44] J. Ge, L. Hu, Y. Song, and S. Jiao, "An investigation into the carbon nucleation and growth on a nickel substrate in $LiCl - Li_2CO_3$ melts," *Faraday discussions*, vol. 190, pp. 259–268, 2016. DOI: https://doi.org/10.1039/C5FD00217F.

[45] E. Medvedovski, "Tin oxide-based ceramics of high density obtained by pressureless sintering," *Ceramics International*, vol. 43, no. 11, pp. 8396–8405, 2017. DOI: https://doi.org/10.1016/j.ceramint.2017.03.185.

[46] H. Yin, X. Mao, D. Tang, *et al.*, "Capture and electrochemical conversion of CO_2 to value-added carbon and oxygen by molten salt electrolysis," *Energy & Environmental Science*, vol. 6, no. 5, pp. 1538–1545, 2013. DOI: https://doi.org/10.1039/C3EE24132G.

[47] S. Jiao and D. J. Fray, "Development of an inert anode for electrowinning in calcium chloride–calcium oxide melts," *Metallurgical and materials transactions B*, vol. 41, no. 1, pp. 74–79, 2010. DOI: https://doi.org/10.1007/s11663-009-9281-8.

[48] S. Jiao, L. Zhang, H. Zhu, and D. J. Fray, "Production of niti shape memory alloys via electro-deoxidation utilizing an inert anode," *Electrochimica acta*, vol. 55, no. 23, pp. 7016–7020, 2010. DOI: https://doi.org/10.1016/j.electacta.2010.06.033.

[49] L. Hu, Y. Song, J. Ge, S. Jiao, and J. Cheng, "Electrochemical metallurgy in $CaCl_2 - CaO$ melts on the basis of $TiO_2 \cdot RuO_2$ inert anode," *Journal of the Electrochemical Society*, vol. 163, no. 3, E33, 2015. DOI: https://doi.org/10.1149/2.0131603jes.

[50] J. E. Randles, "A cathode ray polarograph. part ii.—the current-voltage curves," *Transactions of the Faraday Society*, vol. 44, pp. 327–338, 1948.

[51] R. S. Nicholson and I. Shain, "Theory of stationary electrode polarography. single scan and cyclic methods applied to reversible, irreversible, and kinetic systems.," *Analytical chemistry*, vol. 36, no. 4, pp. 706–723, 1964.

[52] T. Berzins and P. Delahay, "Oscillographic polarographic waves for the reversible deposition of metals on solid electrodes," *Journal of the American Chemical Society*, vol. 75, no. 3, pp. 555–559, 1953. DOI: https://doi.org/10.1021/ja01099a013.

[53] G. Gunawardena, G. Hills, I. Montenegro, and B. Scharifker, "Electrochemical nucleation: Part i. general considerations," *Journal of Electroanalytical Chemistry and Interfacial Electrochemistry*, vol. 138, no. 2, pp. 225–239, 1982. DOI: https://doi.org/10.1016/0022-0728(82)85080-8.

[54] E. A. Ukshe and N. G. Bukun, "The dissolution of metals in fused halides," *Russian Chemical Reviews*, vol. 30, no. 2, pp. 90–107, 1961. DOI: 10.1070/rc1961v030n02abeh002955.

[55] N. Adhoum, J. Bouteillon, D. Dumas, and J. C. Poignet, "Electrochemical insertion of sodium into graphite in molten sodium fluoride at 1025° c," *Electrochimica acta*, vol. 51, no. 25, pp. 5402–5406, 2006.

[56] H. V. Ijije, R. C. Lawrence, N. J. Siambun, *et al.*, "Electro-deposition and re-oxidation of carbon in carbonate-containing molten salts," *Faraday discussions*, vol. 172, pp. 105–116, 2014. DOI: https://doi.org/10.1039/C4FD00046C.

[57] L. Hu, Y. Song, J. Ge, J. Zhu, and S. Jiao, "Capture and electrochemical conversion of CO_2 to ultrathin graphite sheets in $CaCl_2$-based melts," *Journal of Materials Chemistry A*, vol. 3, no. 42, pp. 21 211–21 218, 2015. DOI: https://doi.org/10.1039/C5TA05127D.

[58] Y. Castrillejo, A. Martinez, R. Pardo, and G. Haarberg, "Electrochemical behaviour of magnesium ions in the equimolar $CaCl_2 - NaCl$ mixture at 550°c," *Electrochimica acta*, vol. 42, no. 12, pp. 1869–1876, 1997. DOI: https://doi.org/10.1016/S0013-4686(96)00399-4.

[59] L. Massot, P. Chamelot, F. Bouyer, and P. Taxil, "Studies of carbon nucleation phenomena in molten alkaline fluoride media," *Electrochimica Acta*, vol. 48, no. 5, pp. 465–471, 2003. DOI: https://doi.org/10.1016/S0013-4686(02)00646-1.

[60] F. Lantelme, B. Kaplan, H. Groult, and D. Devilliers, "Mechanism for elemental carbon formation in molecular ionic liquids," *Journal of molecular liquids*, vol. 83, no. 1-3, pp. 255–269, 1999. DOI: https://doi.org/10.1016/S0167-7322(99)00090-2.

[61] K. Aoki, K. Honda, K. Tokuda, and H. Matsuda, "Voltammetry at microcylinder electrodes: Part ii. chronoamperometry," *Journal of electroanalytical chemistry and interfacial electrochemistry*, vol. 186, no. 1-2, pp. 79–86, 1985. DOI: https://doi.org/10.1016/0368-1874(85)85756-7.

[62] I. A. Novoselova, N. F. Oliinyk, A. B. Voronina, and S. V. Volkov, "Electrolytic generation of nano-scale carbon phases with framework structures in molten salts on metal cathodes," *Zeitschrift für Naturforschung A*, vol. 63, no. 7-8, pp. 467–474, 2008. DOI: https://doi.org/10.1515/zna-2008-7-814.

[63] C. W. Bale and E. Bélisle. "Fact-web suite of interactive programs." (2022), [Online]. Available: https://www.crct.polymtl.ca/factweb.php (visited on 05/25/2022).

Appendices

A. Data excluded from the main part

Although the most essential data were presented in Chapter 4, some of them were excluded from the main body of this thesis to enhance the readability. Here, some data are presented as supplementary information.

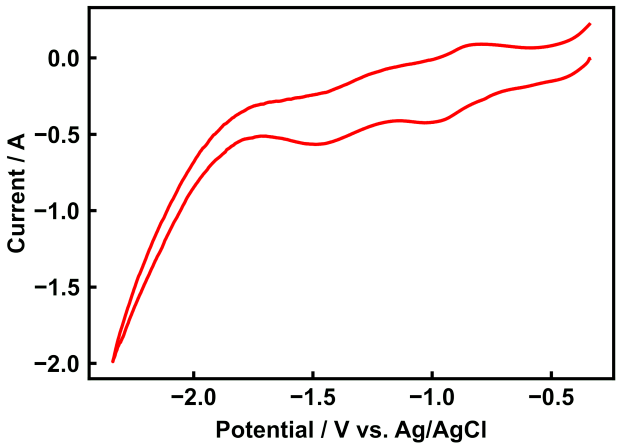

Figure A.1. Typical cyclic voltammogram using a molybdenum working electrode in molten $CaCl_2$-NaCl-$CaCO_3$ (80 mol%:20 mol% + 0.5 mol%). Scan rate: 1000 mV/s. Atmosphere: Ar.

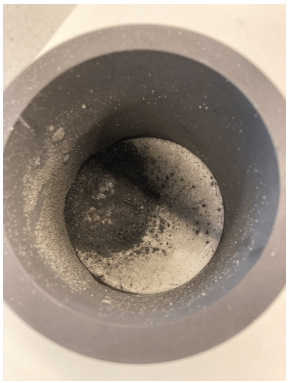

Figure A.2. Photograph of a graphite crucible after prolonged electrolysis of $CaCl_2$-NaCl-$CaCO_3$ molten salt. The place where the carbon product can be seen is the position of the cathode.

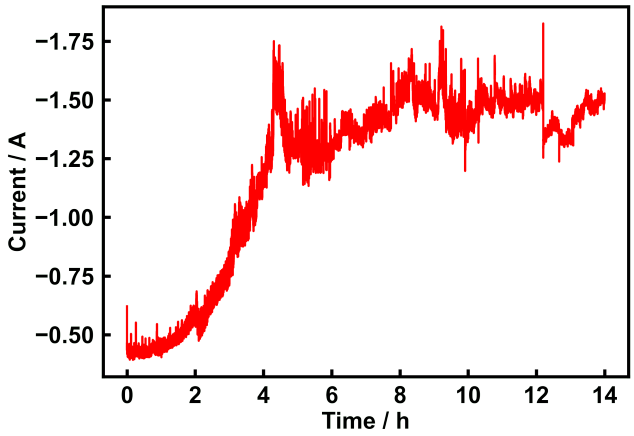

Figure A.3. Potentiostatic electrolysis using a W cathode and a graphite anode at -1.15 V with respect to OCP. Flow gas: pure CO_2, Flow rate: 150 mL/min.

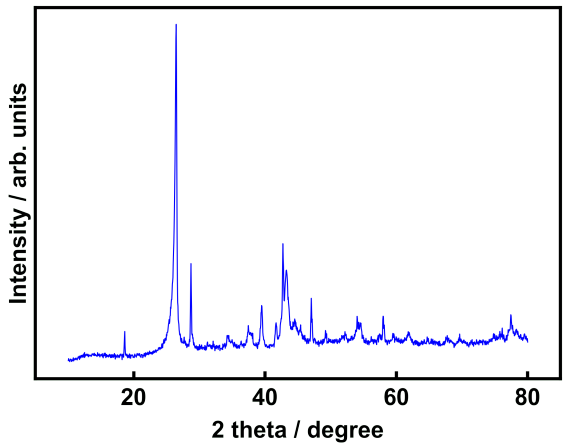

Figure A.4. XRD pattern of the carbon product obtained from potentiostatic electrolysis under pure CO_2 flow. Cathode: W, Anode: graphite, Flow gas: pure CO_2, Flow rate: 150 mL/min.

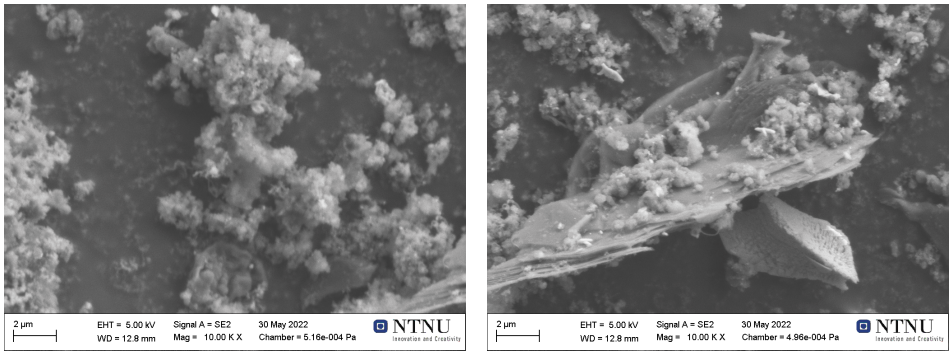

(a) **(b)**

Figure A.5. SEM images of the carbon product obtained from potentiostatic electrolysis under pure CO_2 gas flow. Cathode: W, Anode: graphite. (a) Typical image of the sample and (b) Part including graphitic structures.

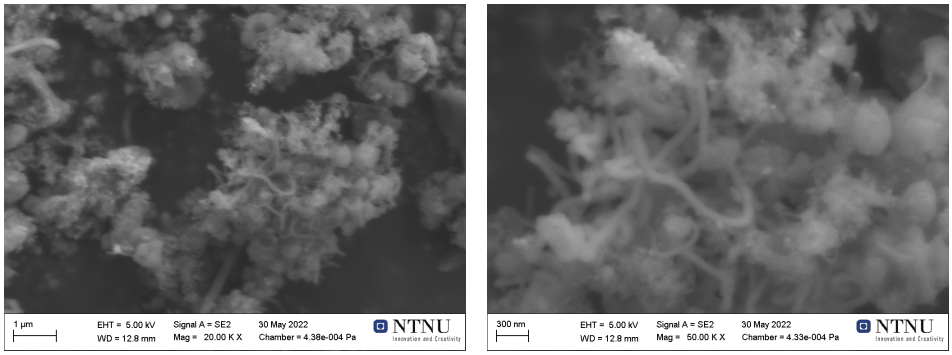

(a) **(b)**

Figure A.6. SEM images of the carbon product obtained from potentiostatic electrolysis under pure CO_2 gas flow. Cathode: W, Anode: graphite. (a) Part including nano-tubular structures and (b) Magnified image.

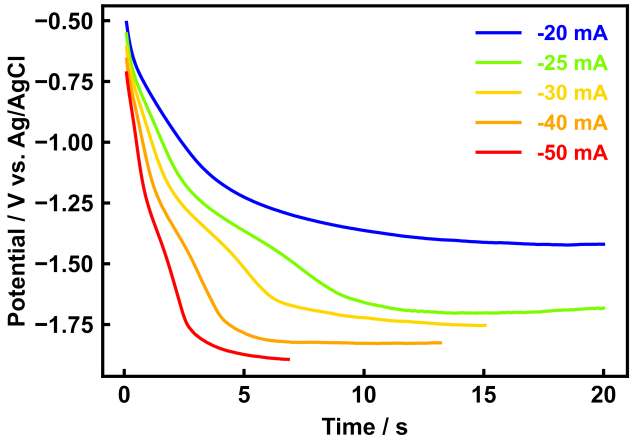

Figure A.7. Chronopotentiograms on a W cathode in molten $CaCl_2$-NaCl-$CaCO_3$ (80:20 mol% + 0.05 mol%). Atmosphere: Ar.

B. Reaction mechanisms of carbon deposition reaction

In Chapter 2, the carbon deposition from carbonate ion was briefly explained. There are three different proposed reaction mechanisms of carbon deposition, and they are introduced here.

(Mechanism 1: One-step electrochemical reduction)

$$CO_3{}^{2-} + 4e^- = C + 3O^{2-}$$

This reaction seems the most widely accepted reaction for the reduction of carbonate into elemental carbon.

(Mechanism 2: Two-step elecrtochemical reduction)

$$CO_3{}^{2-} + 2e^- = CO_2{}^{2-} + O^{2-}$$
$$CO_2{}^{2-} + 2e^- = C + 2O^{2-}$$

We discussed this reaction mechanism in Chapter 4, where the cathodic behaviour of carbonate ion on a W electrode was investigated. The difference from the mechanism 1 is that an intermediate, $CO_2{}^{2-}$ is produced and two electrons are involved in each reaction. Since this intermediate is not very stable, CO can also be formed from $CO_2{}^{2-}$.

$$CO_2{}^{2-} = CO(g) + O^{2-}$$

(Mechanism 2: Electrochemical + metallothermic reduction)

$$M^{n+} + ne^- = M$$

$$2xM + M_xCO_3 = C + 3M_xO$$

In this mechanism, reduction of alkali or alkaline earth metal happens first. The metal can then be dissolved in molten salt and it reacts with carbonate or CO_2 gas. Then, it can be reduced into elemental carbon by metallothermic reduction.

C. Calculation of the standard electrode potentials

In Chapter 2, a table of standard electrode potentials was presented. Those vales were obtained from the Gibbs energy changes calculated with HSC Chemistry (Outotec). Here, the ideas behind it and the detailed procedures are explained.

When we calculate Gibbs energy or electrode potentials, some kind of reference point must be defined. If all the reactions are taking place in an aqueous solution, SHE (Standard Hydrogen Electrode) would be the most suitable and convenient choice. In this $CaCl_2$-based molten salt systems, however, SHE cannot be used due to the absence of hydrogen. So, as the standard, the following reaction was chosen.

$$O_2(g) + 4e^- = 2O^{2-} \quad (E^0 \equiv 0 \text{ [V]}) \tag{1}$$

Here, we assume that this reaction happens at the anode during the electrochemical processes, regardless of the cathodic reactions. Since we have defined this reaction's redox potential as zero, the electrode potential difference can be

$$\Delta E = E_{\text{cathode}} - E_{\text{anode}} = E_{\text{cathode}} \tag{2}$$

Thus, as far as we fix the anodic reaction, it is possible to compare a cathodic electrode potential with others. Now, we will take the carbon deposition reaction as an example and will calculate the standard potential for this reaction.

(Reaction1: Carbon deposition)
The half reaction of carbon deposition from carbonate ions can be expressed as the following equation:

$$CO_3{}^{2-} + 4e^- = C + 3O^{2-} \tag{3}$$

On the other hand, at the anode, reaction (1) is taking place. By adding counter ions (Ca^{2+}) and summing equation (1) and (3) with adjustment of coefficients, the total reaction is

$$CaCO_3 = C + O_2(g) + CaO \tag{4}$$

If we input the above reaction equation in a box in the "Reaction Equations Module" of HSC Chemistry, the Gibbs energy changes will be obtained. Any other databases such as JANAF Thermochemical Tables can be used as well. For instance, at 800°C, $\Delta G = 408.3$ [kJ/mol]. The standard Gibbs energy can be converted with the following relation.

$$E^0 = -\frac{\Delta G^0}{nF} \tag{5}$$

Here, four electrons are involved in the reaction. Thus, n = 4.

$$E^0(\text{Carbon deposition}) = -\frac{408.3 \times 1000[\text{J/mol}]}{4 \times 96485[\text{C/mol}]} = -1.058[\text{V}] \tag{6}$$

Other reactions can be written as follows:
(Reaction2: CO formation)

$$2CaCO_3 = 2CO(g) + O_2(g) + 2CaO \tag{7}$$

(Reaction3: Calcium deposition)

$$2CaO = 2Ca + O_2(g) \tag{8}$$

(Reaction4: Sodium deposition)

$$2Na_2O = 4Na + O_2(g) \tag{9}$$

Here, the coefficients of all the equations are adjusted to make the number of electrons "4". By following the same procedure as the carbon deposition reaction, the electrode potentials of all the other reactions above can also be obtained. The figure C.1 shows the theoretical electrode potentials from 0°C to 1000°C.

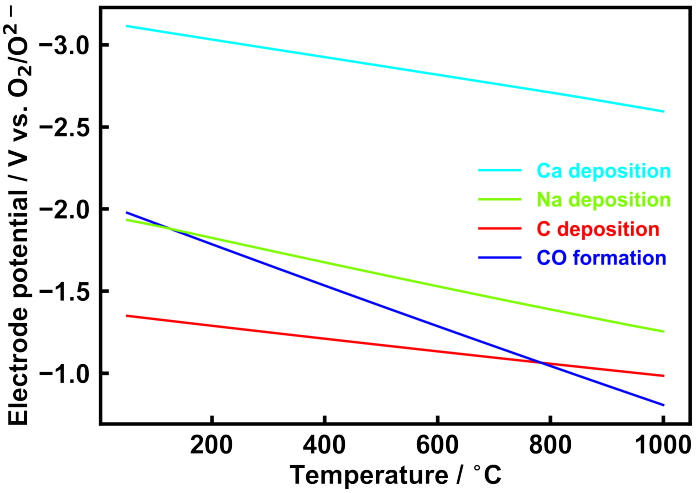

Figure C.1. Standard potentials with respect to the oxygen evolution reaction.

Also, the standard potentials can be different depending on the anodic reactions and the stabilities of the compounds. In Chapter 4, the cathodic behaviour of carbonate was investigated by using $CaCl_2$-NaCl-$CaCO_3$ molten salt. In this case, due to the absence of oxide ions at the initial stage, the standard potentials are somewhat different from the ones presented above. The anodic reaction can be

$$2{CO_3}^{2-} = 2CO_2(g) + O_2(g) + 4e^- \tag{10}$$

Then, the total reactions will be as follows:

(Reaction1: Carbon deposition)

$$3CaCO_3 = C + 2CO_2(g) + O_2(g) + 3CaO \tag{11}$$

(Reaction2: CO formation)

$$4CaCO_3 = 2CO(g) + 2CO_2(g) + O_2(g) + 4CaO \tag{12}$$

(Reaction3: Calcium deposition)

$$2CaCO_3 = 2Ca + 2CO_2(g) + O_2(g) \tag{13}$$

(Reaction4: Sodium deposition)

$$2Na_2CO_3 = 4Na + 2CO_2(g) + O_2(g) \tag{14}$$

By using these equations and the same procedures as before, the results are summarised in Table C.1.

Table C.1: Standard potentials of cathodic reactions at 800°C.

Cathodic reaction	Standard potential / V vs. $CO_3^{2-}/CO_2 - O_2$
$CO_3^{2-} + 4e^- \rightarrow C + 3O^{2-}$	-1.122
$CO_3^{2-} + 2e^- \rightarrow CO(g) + 2O^{2-}$	-1.109
$Ca^{2+} + 2e^- \rightarrow Ca$	-2.773
$Na^+ + e^- \rightarrow Na$	-2.251

If the $CaCl_2$-NaCl system contains neither oxide nor carbonate, the anodic reaction is chlorine evolution.

$$2Cl^- = Cl_2(g) + 2e^- \tag{15}$$

The possible reactions are the following:

(Reaction1: Carbon deposition)

$$CaCO_3 + 2CaCl_2 = C + 2Cl_2(g) + 3CaO \tag{16}$$

(Reaction2: CO formation)

$$CaCO_3 + CaCl_2 = CO(g) + Cl_2(g) + 2CaO \tag{17}$$

(Reaction3: Calcium deposition)

$$CaCl_2 = Ca + Cl_2(g) \tag{18}$$

(Reaction4: Sodium deposition)

$$2NaCl = 2Na + Cl_2(g) \tag{19}$$

The results of the calculation can be summarised below.

Table C.2: Standard potentials of cathodic reactions at 800°C.

Cathodic reaction	Standard potential / V vs. Cl_2/Cl^{2-}
$CO_3^{2-} + 4e^- \rightarrow C + 3O^{2-}$	-1.642
$CO_3^{2-} + 2e^- \rightarrow CO(g) + 2O^{2-}$	-1.628
$Ca^{2+} + 2e^- \rightarrow Ca$	-3.292
$Na^+ + e^- \rightarrow Na$	-3.237

D. Thermodynamic calculation for carbon capture reaction

In order to achieve the carbon recovery process from the atmospheric CO_2 gas, the following reaction is essential.

$$CO_2(g) + O^{2-} = {CO_3}^{2-} \tag{20}$$

If this reaction does not take place as expected, the supply of CO_2 to the cathode will be limited, and it will cause unwanted consequences. Thus, it is important to consider the condition where the carbon capture reaction is maximised. The following thermodynamic calculation is done by using HSC Chemistry (Outotec), according to the total reaction below.

$$CO_2(g) + CaO = CaCO_3 \tag{21}$$

Table D.1: Gibbs energy change and the equilibrium constant at various temperatures.

Temperature / °C	$\Delta_r G^0$ / kJ/mol	K
0	-134.431	5.123×10^{25}
100	-118.460	3.835×10^{16}
200	-102.686	2.174×10^{11}
300	-87.128	8.734×10^{7}
400	-71.782	3.720×10^{5}
500	-56.640	6.714×10^{3}
600	-41.696	3.123×10^{2}
700	-26.945	2.795×10^{1}
800	-12.385	4.008×10^{0}
900	+1.986	8.158×10^{-1}
1000	+16.169	2.171×10^{-1}

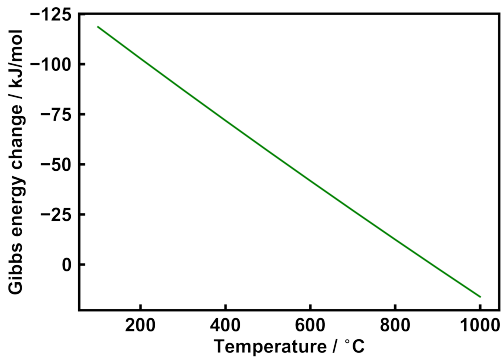

Figure D.1. Gibbs energy change of the reaction as a function of temperature.

E. Detailed dimensions of electrodes and crucibles

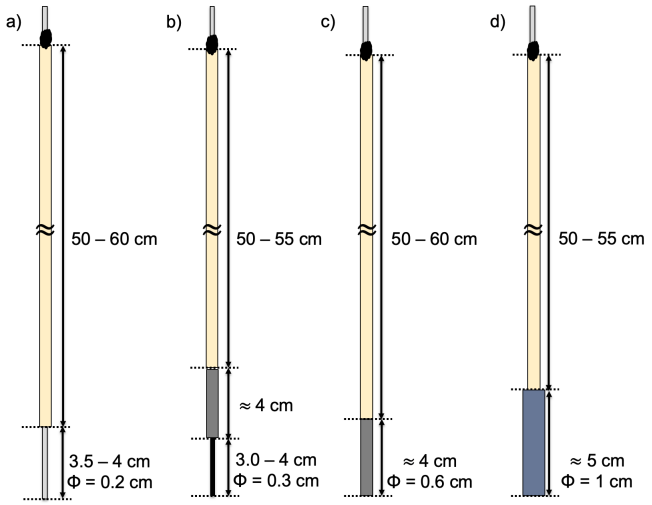

Figure E.1. Dimensions of electrodes used for the experiments: a) W or Mo wire electrode, b) Glassy carbon electrode, c) Graphite electrode, and d) SnO_2-based electrode.

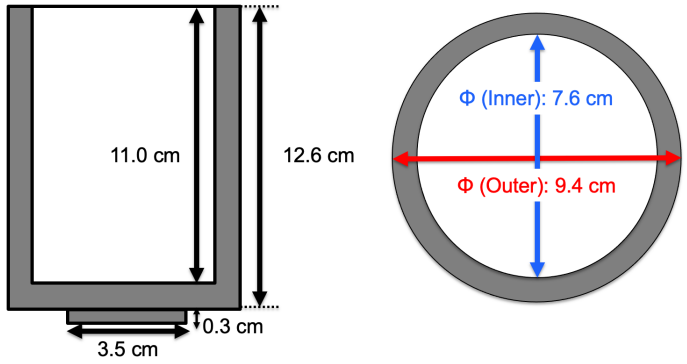

Figure E.2. Dimensions of graphite crucible used for the experiments.

F. How to prepare SnO_2 electrodes

Tin oxide rods are mechanically very hard and it is difficult to make screw holes unlike graphite. So, a somewhat special procedure is needed when we make a hole in it and establish an electrical connection. Here are some recipes for them.

First of all, an ordinary drill cannot machine a tin oxide rod due to its hardness. Thus, a diamond drill or diamond saw is necessary for machining. They are available at the glass workshop in Realfagbygget. There are two ways to attach wires to tin oxide rods.

(Option A) Make a hole with a diamond drill in a tin oxide rod. Since it is very difficult to make a thread, we cannot simply insert and fix a steel rod in it. So, a platinum foil can be sandwiched between the hole and the steel rod (Fig. F.1). This Pt foil makes it possible to tightly attach the rod, and it enhances the mechanical durability and electrical connection.

(Option B) Make a groove around a tin oxide rod. Then, a Pt (or W) wire can be winded along the groove. The wire can be attached to a steel rod so that we could save platinum wires. It is desirable to make a groove on the steel rod as well, in order to avoid the wire slipping off.

It is even possible to combine both Option A and B, which may further improve the connection and provide a redundancy in case some problems occur during experiments.

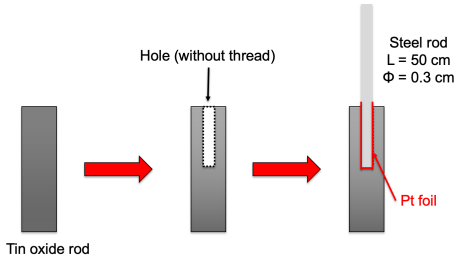

Figure F.1. Option A.

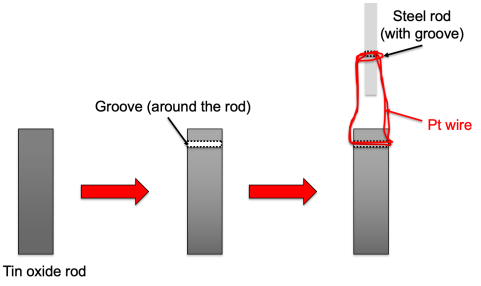

Figure F.2. Option B.

G. Measurement of the surface area of electrodes

Since we cannot see the inside of the furnace during the experiments of molten salt electrochemistry, it is necessary to measure the real surface area of working electrodes in some ways. Here, a way used by the author during this project is introduced.

We assume that the shape of the working electrode is all cylindrical. The length of the electrode dipped in the melt is l[cm], and the radius of the electrode is r[cm]. The surface area of the electrode (A) can be calculated as follows.

$$A = \pi r^2 + 2\pi rl \tag{22}$$

Also, the current (I) that flows through the electrode is proportional to its surface area exposed to the electrolyte.

$$I = kA \tag{23}$$

Here, k is a constant. If we substitute A in the second equation with the first equation, we will get:

$$I = k(\pi r^2 + 2\pi rl) = k\pi r^2 + 2\pi rkl \tag{24}$$

The current is now expressed as the function of the dipped length of the electrode. An I-l plot should look like the following figure:

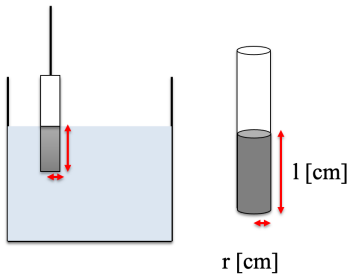

Figure G.1. Electrode dipped in a melt.

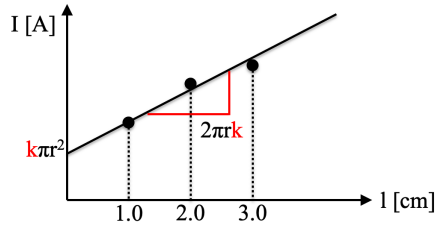

Figure G.2. Typical I - l plot.

The slope is $2\pi rk$ and the intercept is $k\pi r^2$. In principle, the calculated k from the slope and intercept should be exactly the same. But since we normally do not know the exact values of l, we need to use approximated "guesses", which are obtained from a rough measurement using a ruler. When the approximated l values are applied, they will give us two different k values, which indicates that the "guesses" are wrong. However, even if l values are wrong, the slope is always the same and the k obtained from the slope can be trusted. So, what we can do here is to optimise the l values, so that we could get exactly the same k values from the slope and intercept. To optimise l, some sort of programming codes may be utilised. The handiest way would be to use "Goal seek" in Excel.

H. Noise problems during electrochemical measurements

Throughout the semester, the author was suffering from picking up unwanted periodic noises during the electrochemical measurements. Even though the problem was not completely eliminated, it was minimised (or just circumvented) thanks to many people's help. Here, what was tried, what have been found, what the consequences were, and what can be done next will be shared. The author would be happy if this document is helpful for the next person who may use the same setup and struggle with the same problem.

Generally, the origin of noises are very diverse and there is no cure-all. So, it is necessary to take different and appropriate measures from system to system. The following literature was of help in terms of giving the author typical causes of a noise problem: Lifting the lid on the potentiostat: a beginner's guide to understanding electrochemical circuitry and practical operation (DOI: https://doi.org/10.1039/D1CP00661D).

First, Figure H.1 shows a typical profile of the noises that the author experienced. From the sweep rate, the potential range, and the number of noises (pairs), one can easily tell that the frequency of the noise is 50 Hz. So, it can be considered that these noises come from the main power (230 V AC, 50 Hz in Norway).

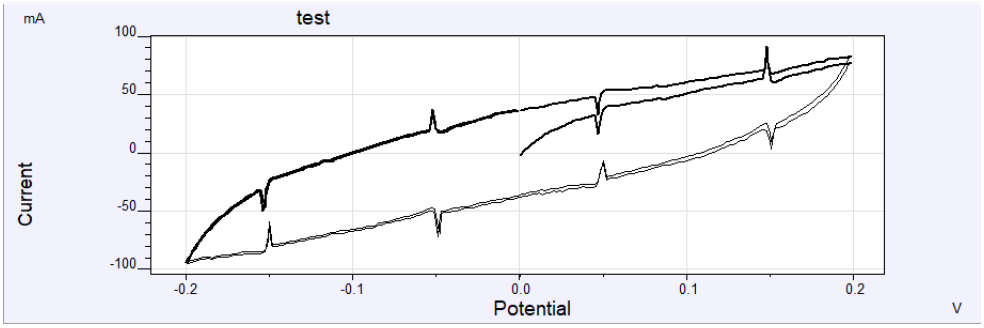

Figure H.1. Typical CV with periodic noises. Scan rate: 10000 mV/s

Since high temperature electrochemical experiments were carried out in an electric furnace, the most probable culprit was clearly the furnace surrounding the cell. The main power is 230 V AC and it is lowered down to 75 V by a transformer inside the temperature controller (Fig H.2). Even periodic beeping sounds were audible when the top lid of the controller was removed. Thus, it was natural to attempt to turn it off temporarily and to compare the profiles with the power on and off.

When the furnace was turned off, the noises became smaller, even though they were not completely eliminated. Therefore, the noise was partly because of the

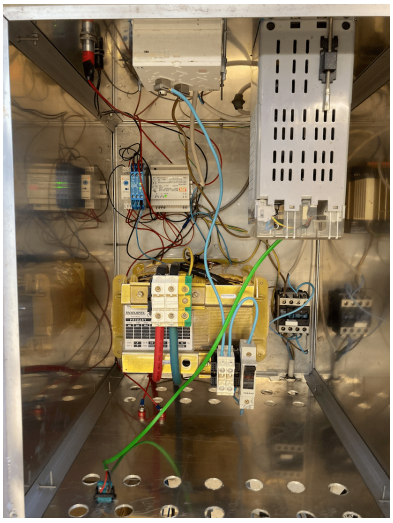

Figure H.2. Photograph of the equipment inside the temperature controller.

electric furnace. Since the cell is surrounded by metal coils to provide resistance heating, AC is flowing when the switch is turned on. It creates an electromagnetic field and can lead to cause the noises.

Another cause of the noise was the high impedance of the reference electrode. If the reference electrode is in a bad shape, such as a corroded wire, some deposition in the frit etc., it results in a high impedance and make the response of the potentiostat slower. Since the state of our reference electrode cannot be observable from the outside (Ag/AgCl reference electrode in a mullite tube), the author broke one of them with a hammer and the state of inside was checked. The author's expectation was that the silver wire inside might be somewhat corroded. But as it turned out, the condition was worse than expected. The silver wire was almost lost and it seemed the electrical connection was barely maintained.(Figure H.3). Although the lifespan of reference electrodes are different from system to system, it is important to remember that they become useless sooner or later, particularly, in the case of molten salt systems. After replacing the reference electrode with a new one, the noise became smaller. If the furnace is also turned off, the noise was completely eliminated.

In order to reduce the frequency to replace the reference electrode, use of quasi-reference electrodes is also an option. They indicate fairly stable potential, are acceptably durable, and are easy to fabricate. However, since we do not know what kind of reaction is happening at the electrode, the potential cannot be defined thermodynamically. Therefore, it is always necessary to measure the potential difference between a "proper" reference electrode and the quasi reference electrode

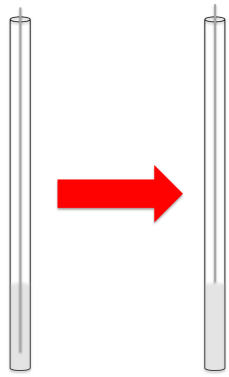

Figure H.3. Illustration of the situation where an Ag wire was almost lost in an Ag/AgCl reference electrode.

so that we could assure the reproducibility.

After all, what the author have been doing to mitigate the noises are summarised below:

(i) Turn off the furnace every time when doing voltammetry. It is important not to forget to turn it on again as the temperature drops easily and it can affect the result.

(ii) Use a "fresh" reference electrode. Ideally, a new one should be made for every experiment. If that is not possible due to the cost or availability, at least make sure to change the silver wire every two or three experiments. As for the diameter of the silver wire, the thicker, the better. If a thick Ag wire cannot be found, at least try to wind the wire and make a coil to make it as durable as possible. To check the state of the silver wire, push the wire down to the bottom of the mullite tube and feel the hardness of the wire. If the wire is corroded badly, it will collapse and you will be able to feel it. Then, after measuring the potential difference from the quasi reference electrode, the Ag/AgCl reference electrode must be retrieved from the system, so that we can maximise its life time.

The following measures were also tried. In theory, they should have improved the situation, but unfortunately, the effectiveness was not confirmed in our case.

(i) Use of an isolation transformer. An isolation transformer is a device to galvanically isolate electronic devices, which allows us to have a different reference ground point from earth. This feature is convenient when the electrochemical system is grounded in some ways. Normally, two different operating modes are selectable in most of potentiostats: floating or grounded mode.(Figure H.4) When the potentiostat is in use in a grounded mode, the electrochemical cell must be floating to avoid

the effect of "ground loop", which can cause huge noises. Although inserting an isolation transformer was attempted in various manners with two operating modes, the results were not as good as hoped.

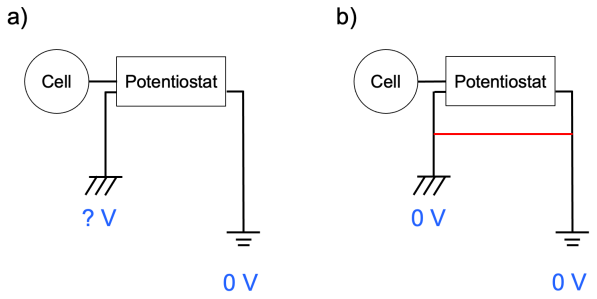

Figure H.4. Two different modes of a potentiostat. a) Floating and b) Grounded mode.

(ii) Make the cables as short as possible. Long cables can be a good antenna for picking up noises. Also, try to avoid using a corroded clips and make sure to polish the connections with sandpapers.

The following countermeasures were also tried. But they did not work well and some of them made the situation worse.

(i) Use of "filters" in the potentiostat was tried. In most potentiostats, digital filters to mitigate noises are available. In an IVIUM-n-STAT, several different lowpass filters can be chosen. Since the noise was 50 Hz, a "10 Hz" filter was attempted. Although it successfully got rid of the noises, the shape of the I-V curve was drastically changed. So, it was no longer raw data and cannot be used for analysis.

(ii) Smoothing function was also attempted. It is also possible to remove the noises from the data by using the IVIUM software. It did not change the data so drastically. However, it is still not ideal to edit the data. Therefore, the author decided not to use this function either.

Followings are the items that the author has not tried yet and are something that may improve the situation in the future work.

(i) Use of shielded cables might be helpful to block the noises. The cables from IVIUM-n-STAT are shielded. But the extensions were not. So, if the cables are replaced with shielded ones, it might be somewhat effective to minimise the noises. However, the length of electrodes are so long in the present experimental set-up, and there is still a possibility to pick the noises up there. In fact, the author changed the position of the potentiostat once and tried not to use any extensions.

But the situation was the same.

(ii) A Faraday cage is generally a good countermeasure to eliminate the noise problems in electrochemistry. However, as far as our setup is concerned, this is not a very realistic way. Since we are doing a high temperature experiment, the cage must be resistant to the high temperature, such as tungsten. Due to the size of the furnace, it will be costly and not easy to fabricate such a large metal tube.

(iii) Use of DC current to heat the furnace instead of AC can be of help. Alternating current has a periodic cycle and it creates a disturbance periodically. But if it is converted into DC by using a rectifier, at least, the disturbance will not be periodic anymore.

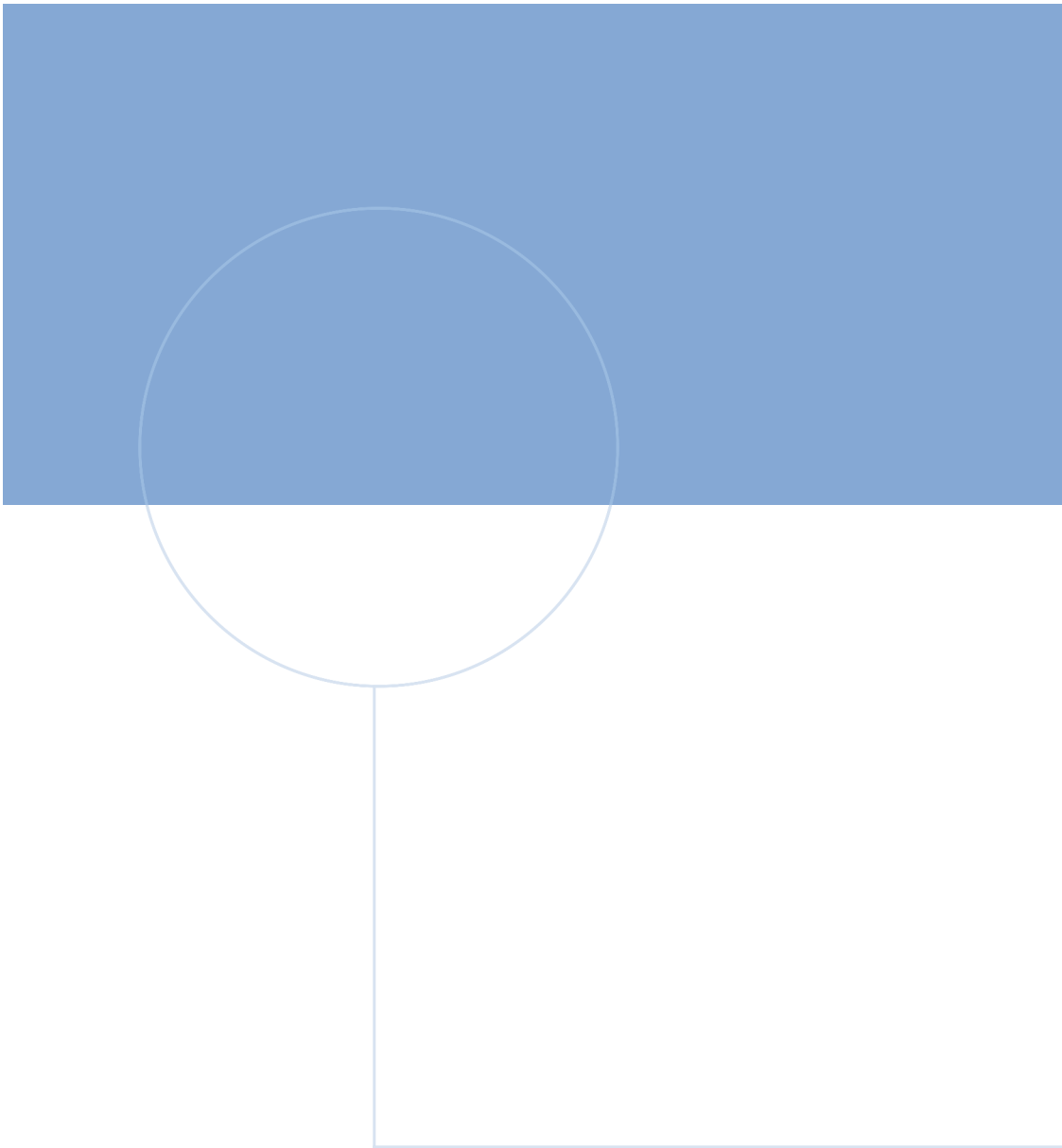

NTNU

Kunnskap for en bedre verden